Chapter-4

Results

Endophytic bacteria hold diverse bioactive compounds which has wide applications in various fields. They selectively favor mutualistic association with the host plant they colonize, and their structure, composition, and diversity are closely related to plant physiology. Moreover, medicinal plants are considered as a store house of beneficial endophytic microorganisms. Research on the biological study of endophytic bacteria in the medicinally important plants reveal that some of the active compounds of pharmaceutical interest present in the plant was also found in the endophytes they carry. Thus the endophytic microorganisms can be used as a substitute for their host plants which have wide medicinal property. Therefore, our present research was focussed on the isolation and beneficial study of endophytic bacteria present in two medicinal plants, *M. citrifolia* and *M. pubescens*. A total of fifteen endophytic bacteria were isolated from the fresh and healthy leaves of these two medicinal plants, *M. citrifolia* (nine isolates) and *M. pubescens* (six isolates). Also, the isolated strains with distinct phenotypes were given code names as shown below.

Fig. 4.1 Schematic representation of code names given to endophytic isolates.

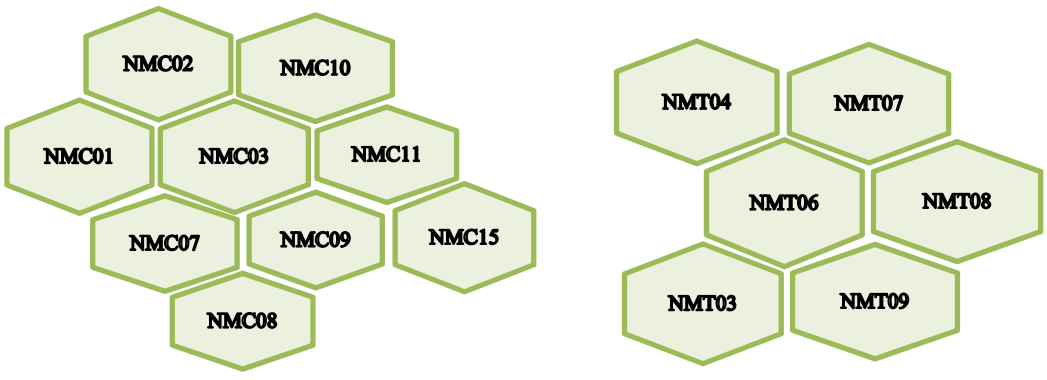

Isolates from *M. citrifolia* **Isolates from *M. pubescens***

Serial dilution method was adopted for successful isolation of endophytes. The dilution factor ranging from 10^{-1} to 10^{-7} was taken and each dilution was plated separately to obtain bacterial colony after effective surface-sterilization method (Fig. 4.2). Antifungal antibiotics were added to the media to reduce the emergence of undesired endophytes, especially fungal groups. The preservation and maintenance of pure culture after constant sub-culturing through streak plate method, was stored in 50% glycerol stock in deep freezer at -20° C.

Fig. 4.2 Photograph showing endophytic bacterial culture from *Morinda* species.

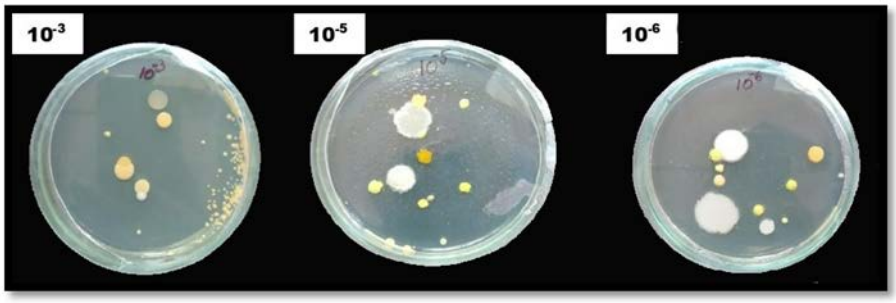

4.1 Identification of endophytic bacteria

4.1.1 Morphological, physiological and biochemical characterization

Traditional phenotypic characterization is necessary with advanced genotypic characterization which is applied using molecular techniques. Usually, microbial isolates were identified through morphological, physiological and biochemical characterization. Microscopic observation revealed that all the fifteen endophytic strains were gram-positive except strain with sample code NMC15 was gram-negative. Distinctive colony characteristics and cellular morphology were mentioned in table 4.1 and table 4.2. The physiological properties for all the isolated strains were documented in table 4.3. The optimum growth temperature of the isolated strains lies in 28° and 37° C and optimum pH in 6 and 7. Biochemical characterization showed that all isolates tests positive for catalase and negative for H_2S production, indole and phenylalanine deaminase test (Table 4.4 and Table 4.5).

Table 4.1 Phenotypic identification of bacteria from *M. citrifolia*.

Characters		NMC01	NMC02	NMC03	NMC07	NMC08	NMC09	NMC10	NMC11	NMC15
Colony characters	Shape/ form	Circular	Slightly irregular	Circular	Circular	Slightly irregular	Circular	Circular	Circular	Circular
	Margin	Entire	Entire	Entire	Entire	Entire	Entire	Entire	Entire	Entire
	Elevation	Raised	Raised	Raised	Raised	Raised	Raised	Raised	Raised	Raised
	Colour	Orange	Light orange	Orange	Yellow	Light yellow	Yellow	Light orange	Bright yellow	Reddish orange
	Texture	Butyrous	Viscid	Mucus	Butyrous	Viscid	Butyrous	Mucus	Butyrous	Mucus
Cell characters	Shape	Bacilli	Bacilli	Bacilli	Cocci	Bacilli	Cocci	Bacilli	Cocci	Bacilli
	Single/ chain	Clusters	Single	Clusters	Irregular clusters	Single	T etrads	Clusters	Tetrads	Clusters
	Motility	Motile	Motile	Motile	Non-motile	Motile	Non-motile	Motile	Non-motile	Motile
	Gram staining	+ve	+ve	+ve	+ve	+ve	+ve	+ve	+ve	-ve
Endospore staining		-ve	+ve	-ve	-ve	+ve	-ve	-ve	-ve	-ve

+ve – Positive –ve – Negative

Table 4.2 Phenotypic identification of bacteria from *M. pubescens*.

Characters		NMT03	NMT04	NMT06	NMT07	NMT08	NMT09
Colony characters	Shape/ Form	Circular	Circular	Circular	Circular	Slightly irregular	Circular
	Margin	Entire	Entire	Entire	Entire	Entire	Entire
	Elevation	Raised	Raised	Raised	Raised	Raised	Raised
	Colour	Bright orange	Yellow	Orange	Dark orange	Light yellow	Lemon yellow
	Texture	Mucus	Butyrous	Mucus	Mucus	Viscid	Mucus
Cell characters	Shape	Bacilli	Cocci	Bacilli	Bacilli	Bacilli	Bacilli
	Single/ Chain	Irregular	Irregular clusters	Single	Single	Single	Irregular
	Motility	Non-motile	Non-motile	Non-motile	Motile	Motile	Motile
	Gram staining	+ve	+ve	+ve	+ve	+ve	+ve
Endospore staining		-ve	-ve	-ve	+ve	+ve	-ve

+ve – Positive –ve - Negative

Table 4.3 Physiological characterization of bacteria from *Morinda* species.

		NMC01	NMC02	NMC03	NMC07	NMC08	NMC09	NMC10	NMC11	NMC15	NMT03	NMT04	NMT06	NMT07	NMT08	NMT09
Growth temperature	**20 ºC**	-	-	-	+	-	+	-	+	-	+	+	+	-	-	+
	28 ºC	+	+	+	++ (*)	+	++ (*)	+	++ (*)	+	++(*)	++ (*)	+	-	+	++(*)
	37 ºC	++ (*)	++ (*)	++ (*)	+	++ (*)	+	++ (*)	+	++ (*)	+	+	++ (*)	++ (*)	++ (*)	+
	40 ºC	-	+	-	+	+	+	-	+	-	-	+	+	+	+	-
Growth pH	**4**	-	-	-	-	-	-	-	-	-	-	-	-	-	-	-
	5	-	+	-	-	+	-	-	-	-	-	-	+	-	+	-
	6	+	++ (*)	+	+	++ (*)	+	+	+	-	++(*)	+	++(*)	-	++ (*)	++(*)
	7	++(*)	+	++(*)	++ (*)	+	++ (*)	++ (*)	++ (*)	++ (*)	+	++ (*)	++	++(*)	+	+
	10	-	-	-	-	-	-	-	-	+	+	-	+	+	-	+

- indicates no growth, + indicates moderate growth, ++ indicates good growth, (*) indicates optimum growth

Table 4.4 Biochemical screening of bacteria from *M. citrifolia*.

		NMC01	NMC02	NMC03	NMC07	NMC08	NMC09	NMC10	NMC11	NMC15
Catalase		+ve	+ve	+ve	+ve	+ve	+ve	+ve	+ve	+ve
Oxidase		+ve	–ve	–ve	–ve	–ve	–ve	+ve	–ve	+ve
Citrate test		–ve	–ve	+ve	–ve	–ve	–ve	–ve	–ve	–ve
KIA	Fermentation	–ve	–ve	–ve	–ve	–ve	–ve	–ve	–ve	–ve
	H_2S production	–ve	–ve	–ve	–ve	–ve	–ve	–ve	–ve	–ve
Indole test		–ve	–ve	–ve	–ve	–ve	–ve	–ve	–ve	–ve
Litmus milk test		–ve	–ve	–ve	–ve	–ve	–ve	–ve	–ve	–ve
Phenylalanine deaminase test		–ve	–ve	–ve	–ve	–ve	–ve	–ve	–ve	–ve
Nitrate reductase		+ve	–ve	–ve	–ve	–ve	–ve	–ve	–ve	–ve
Urease		–ve	–ve	–ve	–ve	–ve	+ve	–ve	–ve	–ve
Voges-Proskauer (VP) test		–ve	–ve	–ve	–ve	–ve	–ve	–ve	–ve	–ve
Methyl red (MR) test		–ve	–ve	–ve	–ve	–ve	–ve	–ve	–ve	–ve

+ve – Positive –ve – Negative

Table 4.5 Biochemical screening of bacteria from *M. pubescens*.

		NMT03	NMT04	NMT06	NMT07	NMT08	NMT09
Catalase		+ve	+ve	+ve	+ve	+ve	+ve
Oxidase		–ve	–ve	–ve	+ve	–ve	–ve
Citrate test		–ve	–ve	+ve	–ve	–ve	–ve
KIA	Fermentation	+ve	+ve	–ve	–ve	–ve	+ve
	H_2S production	–ve	–ve	–ve	–ve	–ve	–ve
Indole test		–ve	–ve	–ve	–ve	–ve	–ve
Litmus milk test		+ve	–ve	+ve	–ve	–ve	+ve
Phenylalanine deaminase test		–ve	–ve	–ve	–ve	–ve	–ve
Nitrate reductase		+ve	–ve	+ve	–ve	–ve	+ve
Urease		–ve	–ve	–ve	–ve	–ve	–ve
Voges-Proskauer (VP) test		–ve	–ve	–ve	+ve	–ve	–ve
Methyl red (MR) test		–ve	–ve	–ve	–ve	–ve	–ve

+ve – Positive –ve - Negative

4.1.2 Genotypic characterization of bacteria

The molecular characterization of the isolated endophytic bacteria were done using 16S rRNA gene sequencing method. Furthermore, the isolates were identified with the sequence of closest phylogenetic neighbour deposited in NCB1 database (Table 4.6).

Table 4.6 Identity percentage of the 16S rRNA gene sequences of the isolates with the NCBI database.

Isolate name	Strain	Accession number	Closest phylogenetic neighbor	Identity %
	Strain	**source:**	***Morinda citrifolia***	
NMC01	NMC1	MH674397	*Exiguobacterium aurantiacum* AN2	94.71
NMC02	TJ	MK749430	*Bacillus* sp. SCSSS02	96.47
NMC03	NVJ	MK466364	*Exiguobacterium* sp. T230	97.64
NMC07	EJJ	MK466363	*Micrococcus* sp. M14	100
NMC08	CDV	MK457698	*Bacillus marisflavi* CP31	100
NMC09	CKJ	MK466365	*Micrococcus* sp. FJFR62	95.72
NMC10	KMJ	MN249557	*Exiguobacterium alkaliphilum* S13	100
NMC11	IKA	MK457699	*Micrococcus yunnanensis* 8G	100
NMC15	JAP	MK646066	*Brevundimonas vesicularis* C5-8	99.92
	Strain	**source:**	***Morinda pubescens***	
NMT03	REGI	MN249643	*Microbacterium kitamiense* AS66	99.36
NMT04	STC	MN267736	*Micrococcus yunnanensis* 994	99.91
NMT06	CVB	MN900637	*Brevibacterium* sp. O1	99.60
NMT07	SMC	MN611233	*Bacillus vietnamensis* KST183	94.70
NMT08	MENA	MN267697	*Bacillus marisflavi* P/W8 AM	99.52
NMT09	REKA	MN249644	*Microbacterium paraoxydans* CF 36	99.51

Fig. 4.3 Photograph showing gel electrophoresis of 16S rRNA gene of the isolates.

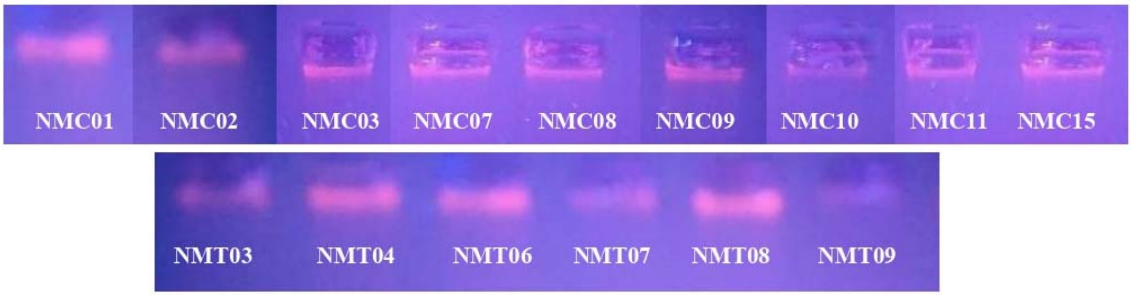

The PCR amplicon of isolates were sequenced and deposited in GenBank as a new strain and got an accession number. The nine strains isolated from *M. citrifolia* are *Exiguobacterium aurantiacum* NMC1 (NMC01), *Bacillus* sp. TJ (NMC02), *Exiguobacterium* sp. NVJ (NMC03), *Micrococcus* sp. EJJ (NMC07), *Bacillus marisflavi* CDV (NMC08), *Micrococcus* sp. CKJ (NMC09), *Exiguobacterium alkaliphilum* KMJ (NMC10), *Micrococcus yunnanensis* IKA (NMC10), *Brevundimonas vesicularis* JAP (NMC15) with accession number MH674397, MK749430, MK466364, MK466363, MK457698, MK466365, MN249557, MK457699, and MK646066, respectively. In contrast, the six strains isolated from *M. pubescens* are *Microbacterium kitamiense* REGI (NMT03), *Micrococcus yunnanensis* STC (NMT04), *Brevibacterium* sp. CVB (NMT06), *Bacillus vietnamensis* SMC (NMT07), *Bacillus marisflavi* MENA (NMT08), *Microbacterium paraoxydans* REKA (NMT09) with accession number MN249643, MN267736, MN900637, MN611233, MN267697, and MN249644, respectively.

Table 4.7 Hierarchical classification of isolated bacterial strains.

	NMC01	NMC02	NMC03	NMC07	NMC08	NMC09	NMC10	NMC11	NMC15
P	Firmicutes	Firmicutes	Firmicutes	Actinobacteria	Firmicutes	Actinobacteria	Firmicutes	Actinobacteria	Proteobacteria
C	Bacilli	Bacilli	Bacilli	Actinobacteria	Bacilli	Actinobacteria	Bacilli	Actinobacteria	α-proteobacteria
O	Bacillales	Bacillales	Bacillales	Micrococcales	Bacillales	Micrococcales	Bacillales	Micrococcales	Caulobacterales
F	Bacillaceae	Bacillaceae	Bacillaceae	Micrococcaceae	Bacillaceae	Micrococcaceae	Bacillaceae	Micrococcaceae	Caulobacteraceae
G	*Exiguobacterium*	*Bacillus*	*Exiguobacterium*	*Micrococcus*	*Bacillus*	*Micrococcus*	*Exiguobacterium*	*Micrococcus*	*Brevundimonas*
S	*aurantiacum*	-	-	-	*marisflavi*	-	*alkaliphilum*	*yunnanensis*	*vesicularis*

	NMT03	NMT04	NMT06	NMT07	NMT08	NMT09
P	Actinobacteria	Actinobacteria	Actinobacteria	Firmicutes	Firmicutes	Actinobacteria
C	Actinobacteria	Actinobacteria	Actinobacteria	Bacilli	Bacilli	Actinobacteria
O	Micrococcales	Micrococcales	Micrococcales	Bacillales	Bacillales	Micrococcales
F	Microbacteriaceae	Micrococcaceae	Brevibacteriaceae	Bacillaceae	Bacillaceae	Micrococcaceae
G	*Microbacterium*	*Micrococcus*	*Brevibacterium*	*Bacillus*	*Bacillus*	*Micrococcus*
S	*Kitamiense*	*yunnanensis*	-	*vietnamensis*	*marisflavi*	-

P- Phylum, C- Class, O- Order, F- Family, G- Genus, S- species

Classification according to Bergey's manual of systematic bacteriology

(Brenner *et al*., 2005; Vos *et al*., 2011; Goodfellow *et al*., 2012)

4.1.2.1 Phylogenetic position of isolated bacterial strains

Phylogenetic trees were constructed using the sequences showing maximum homology with the obtained consensus sequence of the isolates deposited in NCBI GenBank by BLAST analysis. At least, 10 GenBank submitted data were taken to construct a phylogenetic tree in determining the proper phylogenetic position of isolated strain. The fig. 4.4 represents the phylogenetic position of all endophytic bacterial strains isolated from *M. citrifolia* and *M. pubescens*.

Fig. 4.4 Phylogenetic tree of endophytic isolates from *Morinda* species.

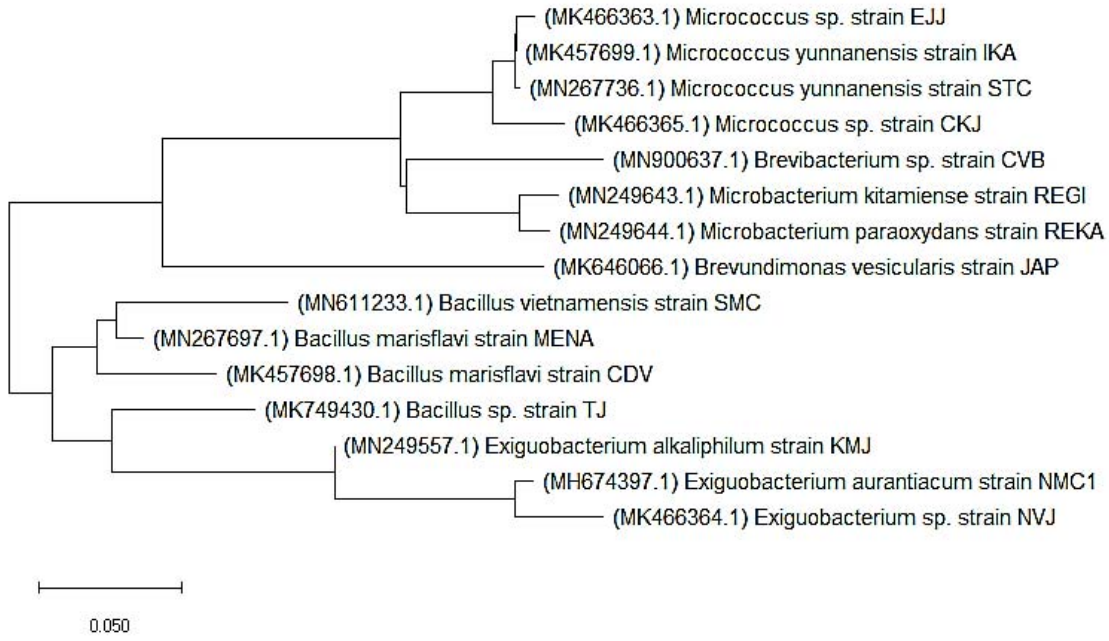

The strain with sample code NMC01 was identified and submitted to GenBank as a new strain of *Exiguobacterium aurantiacum* NMC1 that showed 94.71% sequence homology with strains *Exiguobacterium aurantiacum* and other related strains. In contrast, isolate NMC03 is proposed as *Exiguobacterium* sp., and it showed 97.64% similarity with *Exiguobacterium* sp. T230 and other related species. Isolate NMC10 was identified as *Exiguobacterium alkaliphilum*. The gene sequence was submitted

to GenBank as it showed 100% similarity with *Exiguobacterium alkaliphilum* S13 (Fig.4.5).

Fig. 4.5 Phylogenetic tree of isolated strains of *Exiguobacterium* sp.

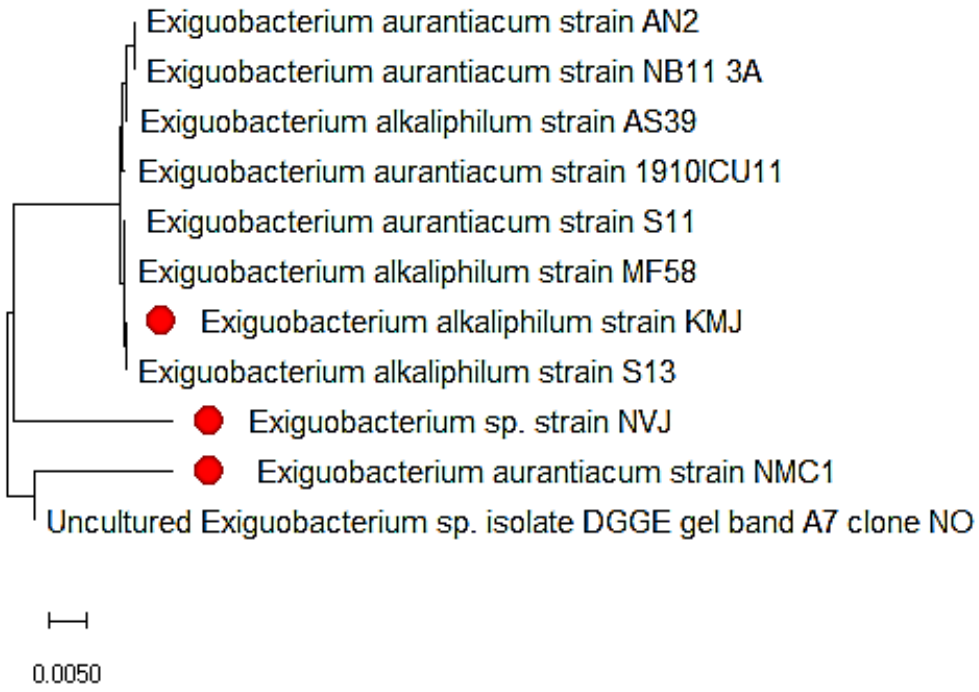

The isolate NMC02 was identified and submitted to GenBank as a new strain *Bacillus* sp. TJ showed 96.47% sequence homology with *Bacillus* sp. and other related strains. In contrast, isolates NMC08 and NMT08 were submitted as *Bacillus marisflavi* CDV and *Bacillus marisflavi* MENA, respectively. In addition, the isolate NMC08 pointed 100% similarity with *Bacillus marisflavi* CP31 and NMT08 (99.52%) with *Bacillus marisflavi* P/W8 AM. Moreover, another *Bacillus* species of isolate NMT07 identified and submitted as *Bacillus vietnamensis* SMC, having 94.70% similarity with *Bacillus vietnamensis* KST183 (Fig. 4.6).

Fig. 4.6 Phylogenetic tree of isolated strains of *Bacillus* sp.

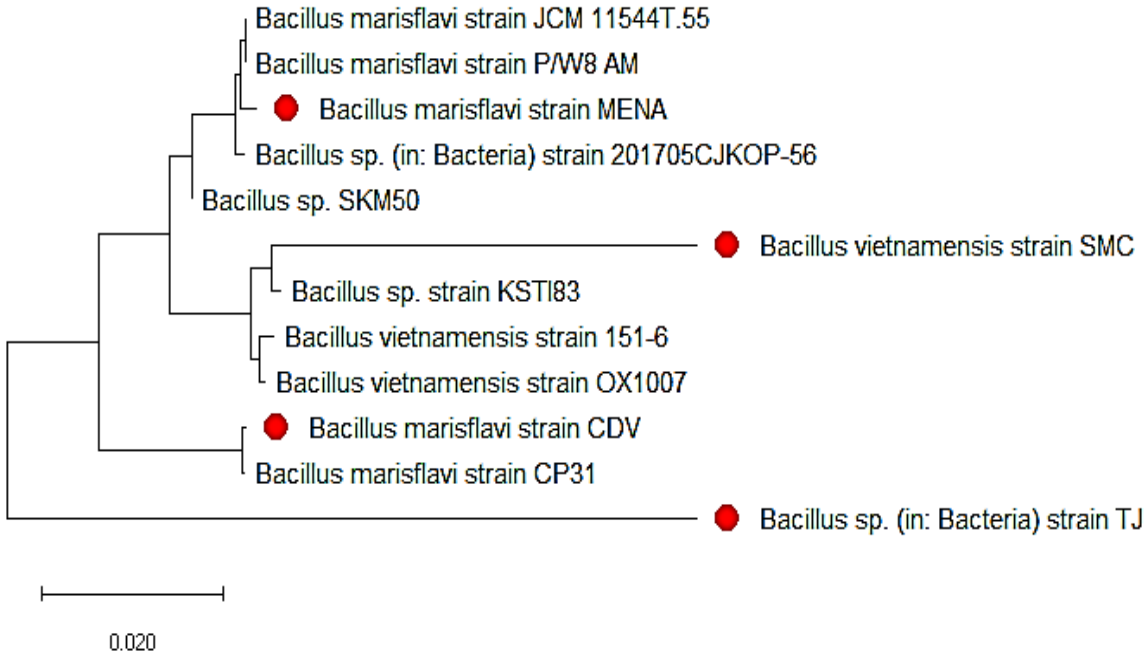

Endophytic isolates NMC07 and NMC09 isolated from surface-sterilized leaves of *M. citrifolia* L. were submitted to GenBank as new strains *Micrococcus* sp. EJJ and *Micrococcus* sp. CKJ showed 100 and 95.72 % sequence homology with *Micrococcus* sp. M14 and other related species, respectively. Further, the isolates NMC11 and NMT04 sequences were identified as *Micrococcus yunnanensis* IKA and *Micrococcus yunnanensis* STC that marked 100% similarity with *Micrococcus yunnanensis* 8G and 99.91% with *Micrococcus yunnanensis* 994 (Fig. 4.7).

Fig. 4.7 Phylogenetic tree of isolated strains of *Micrococcus* sp.

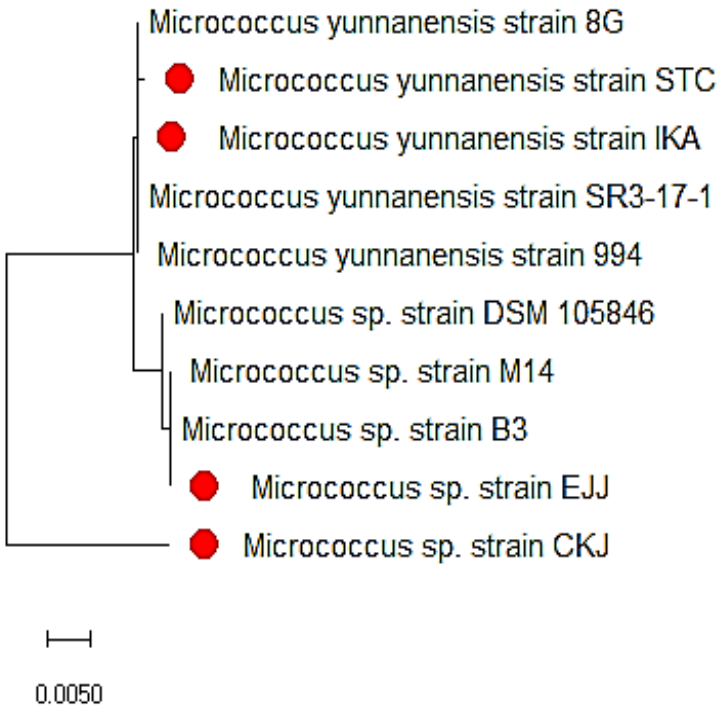

NMC15 isolated from surface-sterilized leaves of *M. citrifolia* L. was submitted to GenBank as new strains *Brevundimonas vesicularis* JAP showed 99.92% sequence homology with *Brevundimonas vesicularis* C5-8 and other related species (Fig. 4.8). Further, the isolates NMT03 and NMT09 sequences were identified as *Microbacterium kitamiense* REGI and *Microbacterium paraoxydans* REKA that marked 99.36% similarity with *Microbacterium kitamiense* AS66 and 99.51% with *Microbacterium paraoxydans* CF 36, respectively (Fig. 4.9). Isolate NMT06 was identified as *Brevibacterium* sp. The submitted 16S rRNA gene sequence to GenBank showed 99.60% similarity with *Brevibacterium* sp. O1 (Fig. 4.10).

Fig. 4.8 Phylogenetic tree of isolated strains of *Brevundimonas* sp.

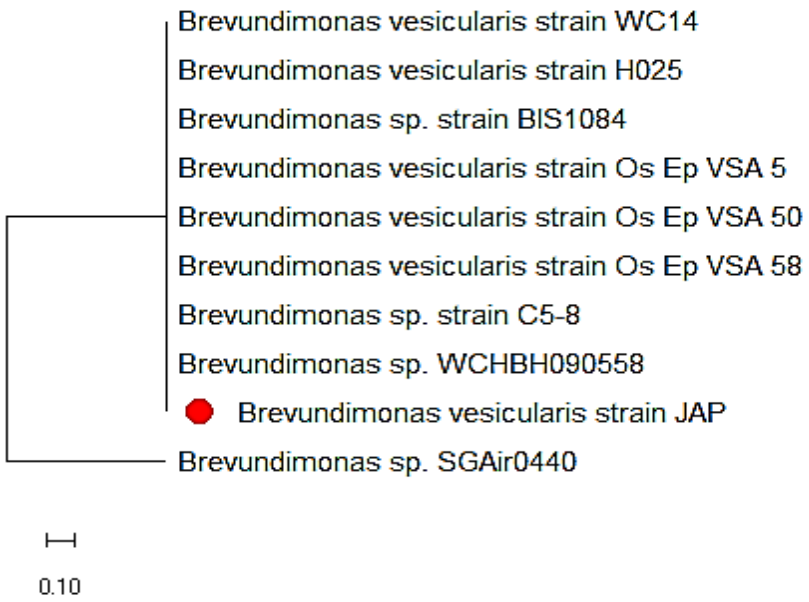

Fig. 4.9 Phylogenetic tree of isolated strains of *Microbacterium* sp.

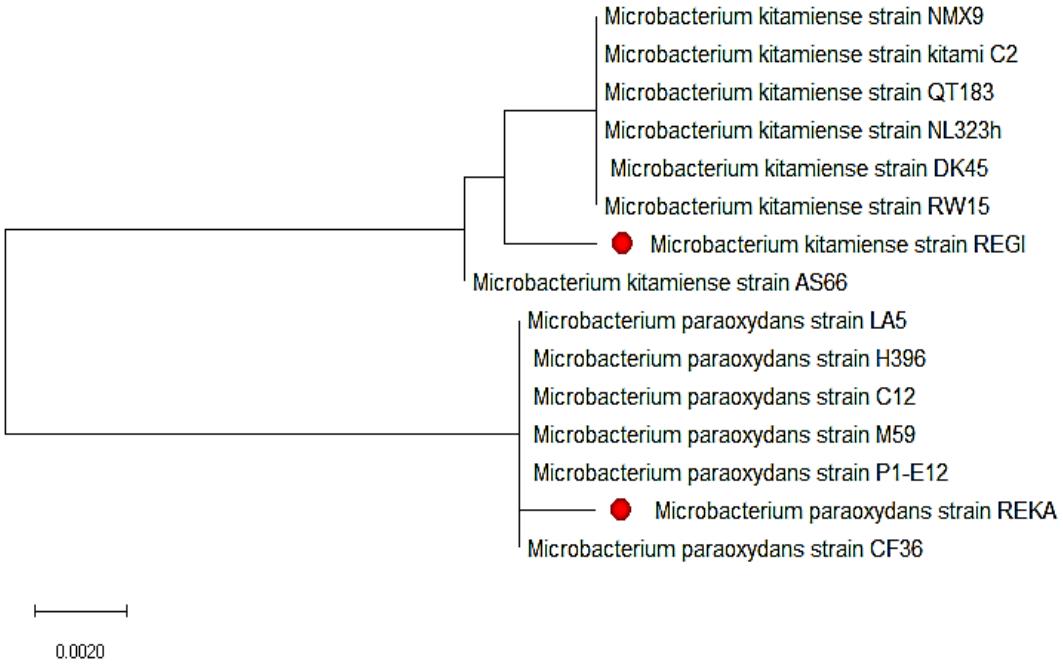

Fig. 4.10 Phylogenetic tree of isolated strains of *Brevibacterium* sp.

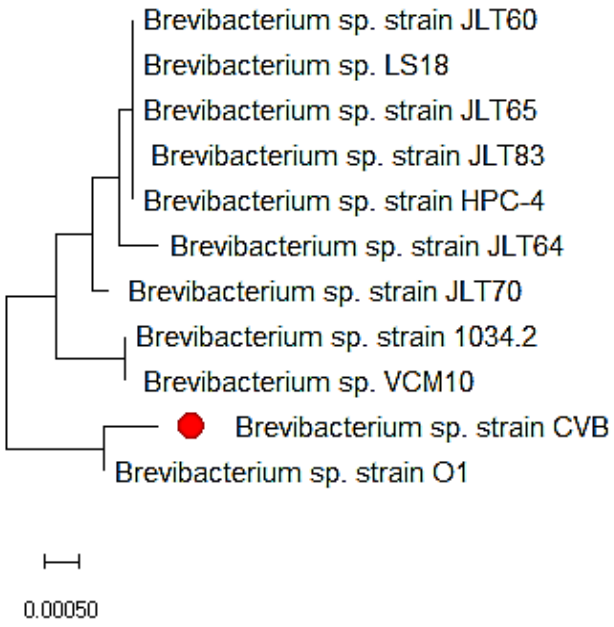

4.2 Metagenomic study on bacterial community and diversity

As there are reports on the metagenome analysis of the endophytic bacterial community in *M. citrifolia,* the present study have focussed on the metagenomic analysis of the endophytic bacterial strains from the leaves *M. pubescens*. The study profiles the complete data about the composition and diversity of microbial community by accessing PCR amplicon of 16S rDNA sequences in the V3-V4 regions. The extracted DNA at absorbance 260/280 nm was 1.89, found to be pure using

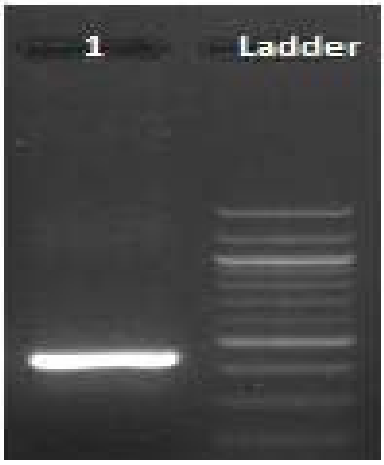

Fig. 4.11 Gel profile of bacterial PCR amplicon.

4.2.1 Sequence data analysis

The paired-end reads obtained from the sample (NMT) were in the format of two FASTq files labelled as NMT_R1.FASTq and NMT_R2.FASTq. Also, it was noted that more than 80% of the total reads have Phred score greater than (>Q30) as shown in fig. 4.12.

Fig. 4.12 Graphical representation of base quality distribution for Read 1 and Read 2 of sample NMT.

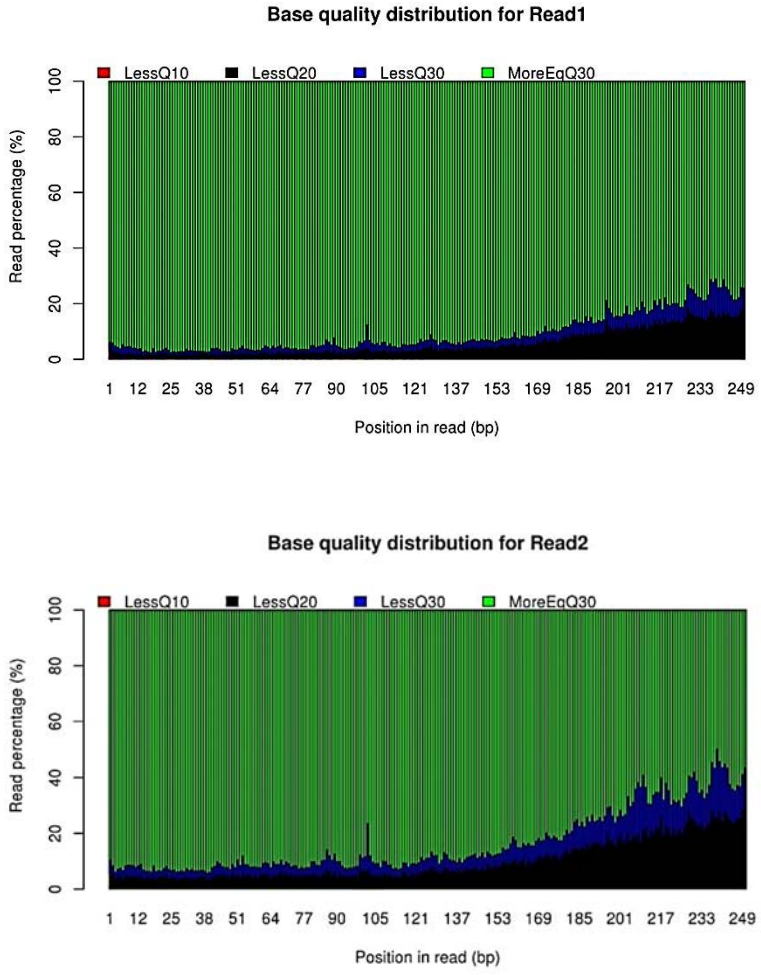

The composition of nucleotides in the sequence read for each sample is shown in fig.4.13. The x-axis represents the sequencing cycle, and the y-axis represents the nucleotide percentage. The adenine, cytosine, guanine, and thymine base

composition distribution of the reads is 22.12, 27.33, 27.16, and 23.33 %, respectively.

Fig.4.13 Sequencing chromatograms of Read 1 and Read 2 of sample NMT.

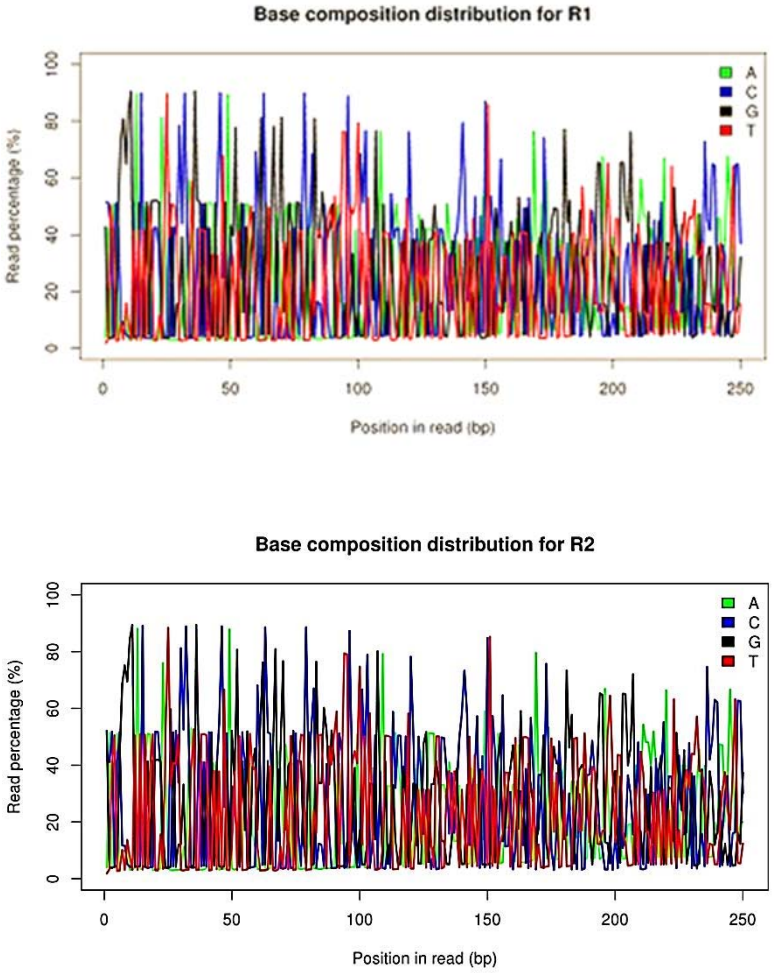

The BioProject (PRJNA516334) was registered with the NCBI GenBank, with the Biosample accession number SAMN10787442. Using the Illumina Hiseq sequencing platform, the consensus sequences obtained is 374752 from the sample NMT. The GC content of the sequence is 54.49. All the consensus sequences formed after removing unwanted sequences have an average contig length of approximately 350-450 bp (Fig. 4.14). The reads after the withdrawal of chimeras using UCHIME tool from 373823 pre-processed sequences were compiled and clustered into Operational

taxonomic units using UCLUST algorithm. A sum total of 198830 OTUs were analyzed from pre-processed sequences out of which 187589 singletons were removed and finally 11241 operational taxonomic units were selected for the taxonomic classification as mentioned in table 4.8.

Fig. 4.14 Contig length distribution of the sequence of sample NMT.

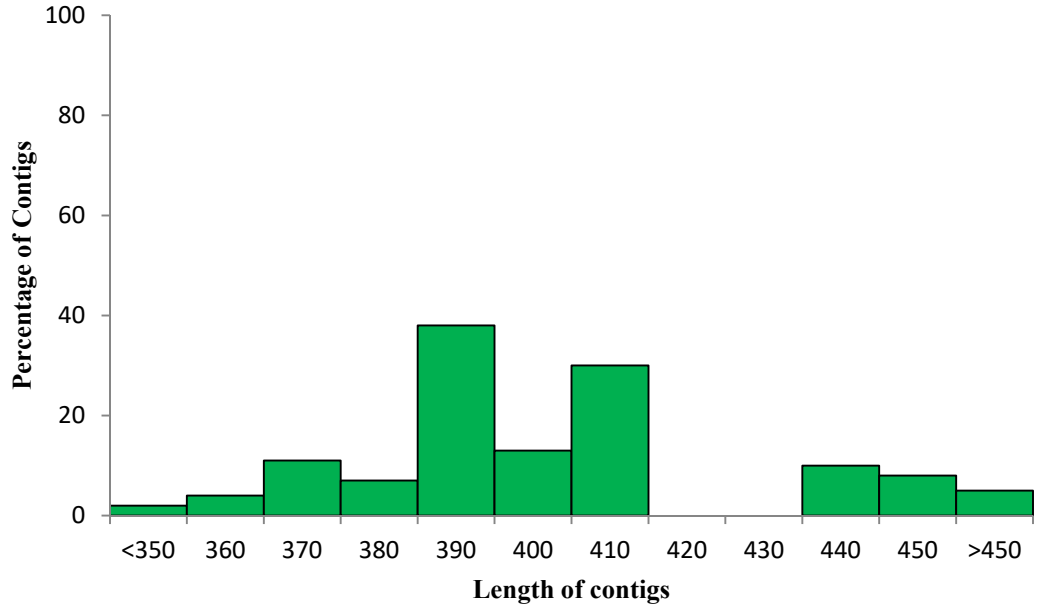

Table 4.8 Summary of OTUs clustered from pre-processed sequences of sample NMT.

Consensus sequences	374752
Chimeric sequences	929
Total Pre-processed Consensus	373823
Total OTUs Picked	198830
Total Singleton OTUs	187589
Total OTUs after Singleton removal	11241

4.2.2 Characterization of bacterial community

The two pipelines MG-RAST and QIIME were used in this study to process the forward and the reverse sequences with the high-demand computational software package. In addition, the taxonomic classification from phylum to the genus of all the OTUs sequences were performed according to the program QIIME and RDP classifier against the SILVA OTUs database.

The obtained raw data pointed that the reads covered the V3-V4 region successfully with an average size of ~250 bp. The result shows the dominance of four important phyla, Proteobacteria, Bacteroides, Firmicutes, and Actinobacteria. Also, OTU distribution summarized the genera; *Brevundimonas*, *Bacteroides*, *Serratia*, and *Propionibacterium* are prevalent in this plant (Fig. 4.15 and 4.16).

Fig 4.15 Graphical representation of OTUs classification at the phylum level of sample NMT.

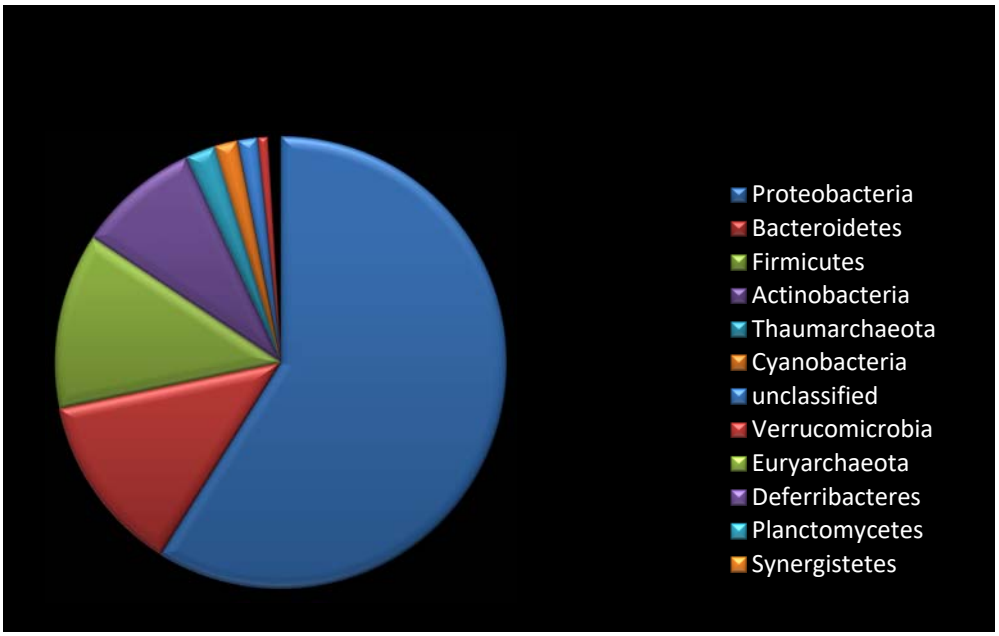

Fig 4.16 Graphical representation of OTUs classification at the genus level of sample NMT.

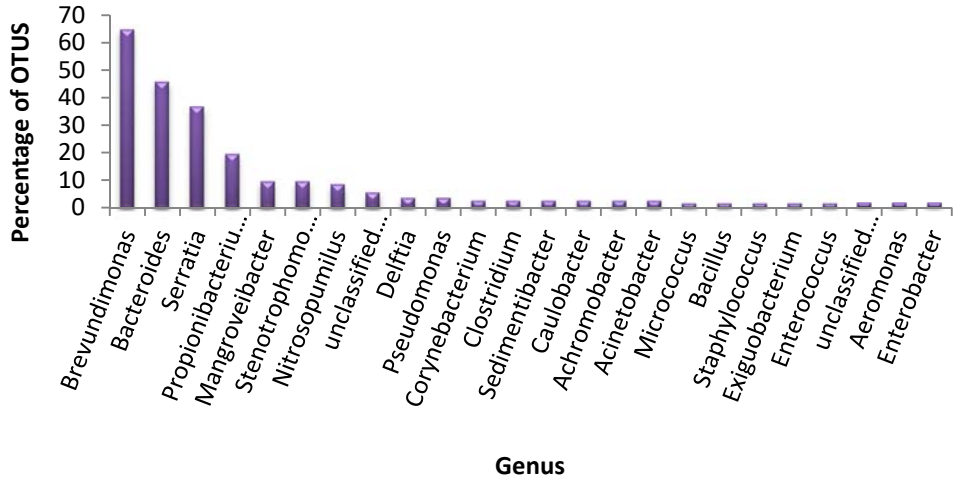

NGS uses the shotgun 16S rRNA gene sequencing, which discloses microbial communities' overall richness and diversity in plant tissues. The α-diversity analysis of the data done in PRIMER 7 software indicates the richness and diversity of the bacterial endophyte belonging to the most prominent phyla were shown in table 4.9. The result indicates the species richness and evenness varies with different phyla.

Table 4.9 Diversity indices among different major phyla.

Phylum	Margalef index (d)	Evenness J'	Shannon diversity index H' (loge)	Simpson index (1-λ)
Proteobacteria	0.7411	0.9975	1.383	0.7616
Bacteroidetes	0.8936	0.8936	1.386	0.7771
Firmicutes	0.9334	0.9334	1.349	0.7642
Actinobacteria	0.9551	0.9551	1.385	0.7834

4.3 Extraction of compounds and GC-MS analysis

Eight bacterial isolates were selected for the extraction of bioactive compounds, as shown in fig. 4.17. The samples lyophilized (Fig. 4.18) were dissolved in ethyl

alcohol for GC-MS profiling to analyze bioactive volatile organic compounds of biological interest.

Fig. 4.17 Plates showing endophytic bacterial isolates selected for the study.

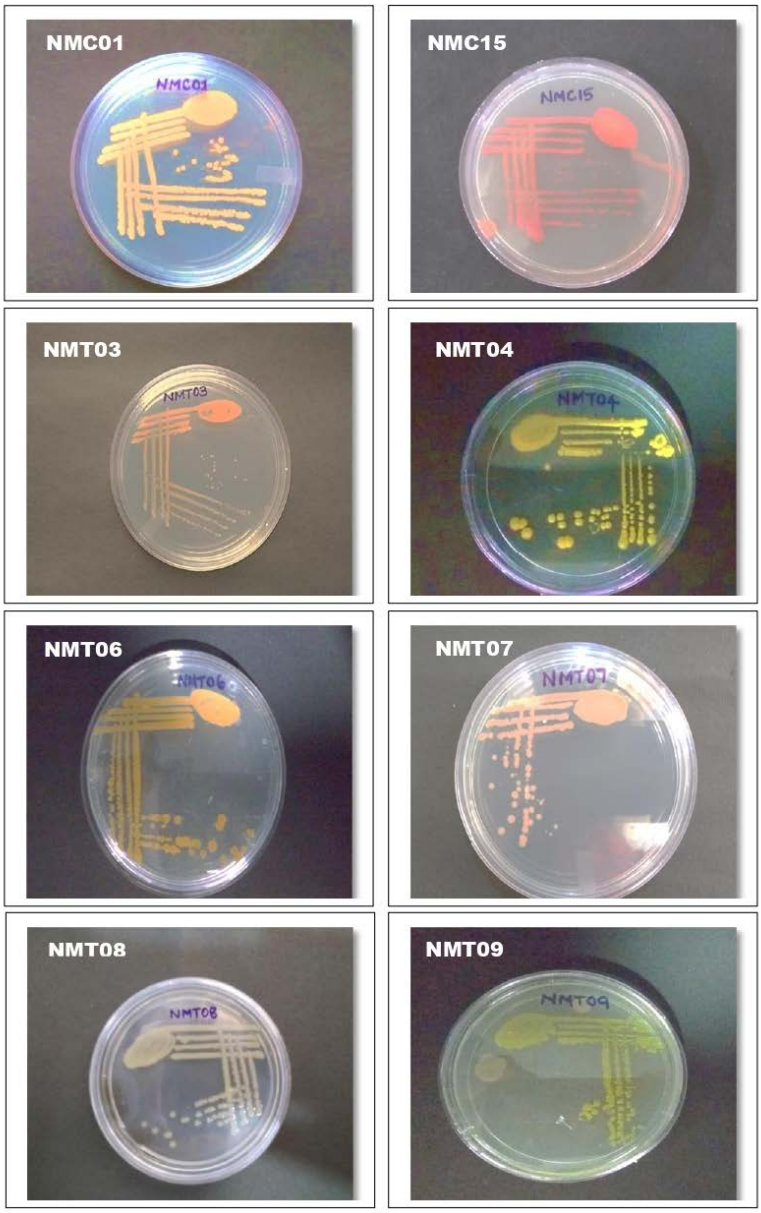

The culture supernatants of the selected isolates were extracted in ethyl acetate solvent. Then, the extract was evaporated using a rota evaporator and reconstituted in ethyl alcohol. Further, ethyl alcohol extracts were lyophilized using freeze drying lyophilizer to get an appropriate measurable amount of extract for the scientific studies in the present work.

Fig. 4.18 Photograph of lyophilised ethyl alcohol extracts of selected samples.

The qualitative study of the compounds present in the ethyl alcohol extract was determined by GC-MS analysis. In the study, chemo-profiling of all the extract of selected isolates were performed. The GC-MS chromatogram and compounds with molecular formula and molecular weight present in all sample extract were figured out (Fig. 4.19 to Fig. 4.26) and tabulated (Table 4.10 to Table 4.17). The major compound present in *Exiguobacterium aurantiacum* NMC1 (NMC01) is cyclo(leucylprolyl) with a peak area of 25.45% and in *Brevundimonas vesicularis* JAP (NMC15) is dicarpyl phthalate with a 58.74% peak area. The primary compound in *Microbacterium kitamiense* REGI (NMT03), *Micrococcus yunnanensis* STC (NMT04), *Bacillus vietnamensis* SMC (NMT07), are 1-Ethylsilatrane (38.11%), 2,4-ditert-butylphenol (62.87%), Dibutyl Phthalate (24.57%), respectively. 1,2-Benzenedicarboxylic acid is the main compound present in *Brevibacterium* sp. CVB (NMT06), *Bacillus marisflavi* MENA (NMT08), and *Microbacterium paraoxydans* REKA (NMT09) with peak area 60.33, 27.14 and 58.89 %, respectively.

Fig. 4.19 GC-MS chromatogram of ethyl alcohol extract of sample NMC01.

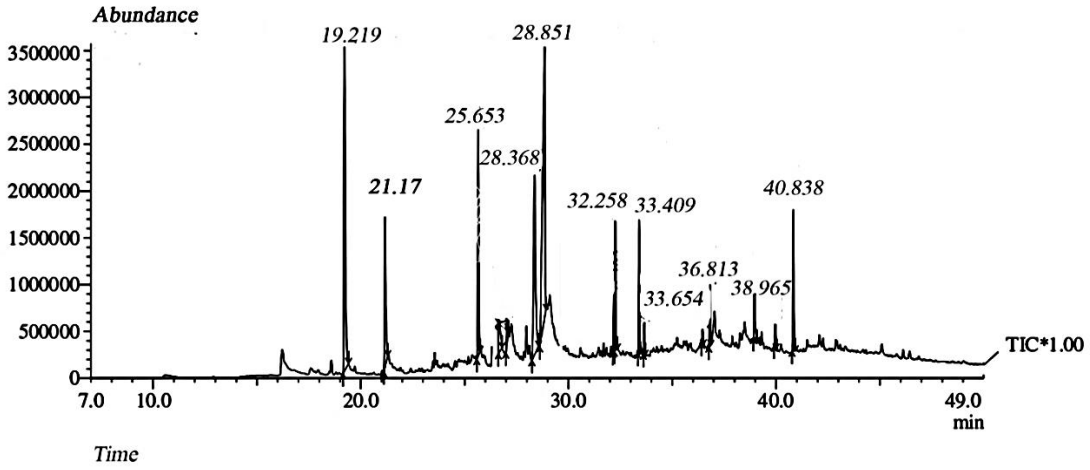

Table 4.10 GC-MS analysis of ethyl alcohol extract of sample NMC01.

RT(mins)	Peak area %	Name of the compound	Molecular formula	Molecular weight
19.219	17.71	Phenol, 2,4-bis(1,1-Dimethyl ethyl)-6-(1-phenylethyl)	$C_{22}H_{30}O$	310.47
21.170	7.34	E-14-Hexadecenal	$C_{16}H_{30}O$	238. 41
25.653	8.52	E-15-Heptadecenal	$C_{17}H_{32}O$	252.44
26.733	2.71	Phenol, 2-(6-hydrazino3-pyridazinyl)	$C_{10}H_{10}N_4O$	202.21
27.036	1.16	Isobutyl phthalate	$C_{12}H_{13}O_4^-$	221.23
28.368	14.65	3-Isobutyl hexahydropyrrolo(1,2-A)pyrazine-1,4-dione	$C_{11}H_{18}N_2O_2$	210.27
28.851	25.45	cyclo(leucylprolyl)	$C_{11}H_{18}N_2O_2$	210.27
32.185	1.77	Octadecanoic acid, Methyl ester	$C_{19}H_{36}O_2$	298.50
32.258	4.63	1-allyl-2,8,9-Trioxa-5-aza-1-silabicyclo(3.3.3)undecane	$C_9H_{17}NO_3Si$	215.32
33.409	4.47	1-Tricosene	$C_{23}H_{46}$	322.61
33.654	1.06	1-Hexadecanol, acetate	$C_{18}H_{36}O_2$	284.48
36.455	0.52	Benzimidazole, 6-(4-diethyl-aminobenzylidenamino)-2-methyl	$C_8H_8N_2$	306.40
36.813	1.95	Heptadecyl trifluoroacetate	$C_{19}H_{35}F_3O_2$	352.48
38.965	1.89	1,2-Benezenedicarboxylic acid	$C_8H_6O_4$	166.13
39.956	0.89	Octadecyl trifluoroacetate	$C_{20}H_{37}F_3O_2$	366.50
40.838	5.28	4,4'-((P-phenylene)-diisopropylidiene dipphenol	$C_{24}H_{26}O_2$	346.46
	100			

Fig. 4.20 GC-MS chromatogram of ethyl alcohol extract of sample NMC15.

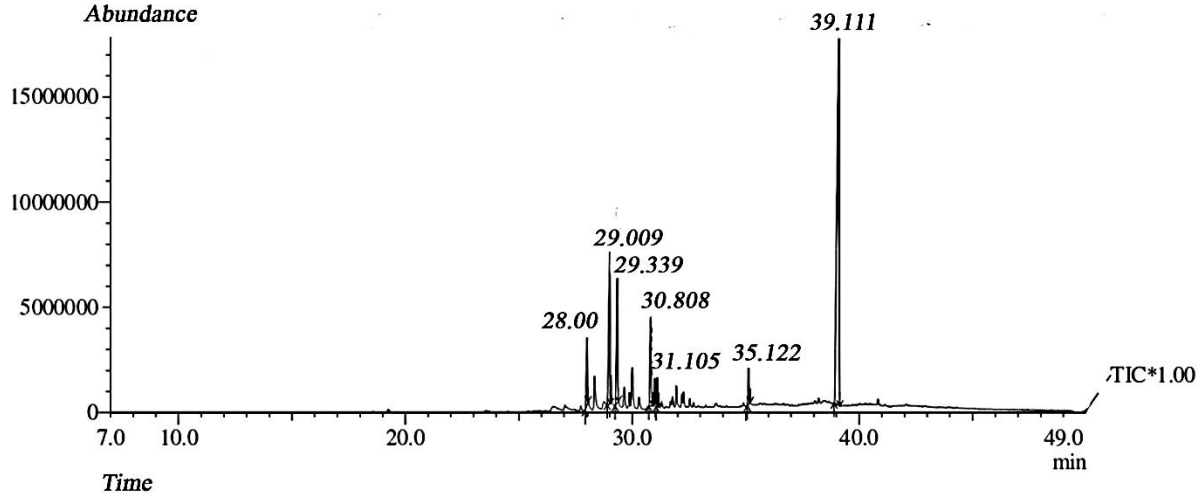

Table 4.11 GC-MS analysis of ethyl alcohol of extract NMC15.

RT(mins)	Peak area %	Name of the compound	Molecular formula	Molecular weight
28.001	4.73	Isobutyl phthalate	$C_{12}H_{13}O_4^-$	221.23
29.009	15.07	Butyl isobutyl phthalate	$C_{16}H_{22}O_4$	278.34
29.339	9.86	Dibutyl phthalate	$C_{16}H_{22}O_4$	278.34
30.808	6.99	Bismethylglycol	$C_8H_{14}O$	90.18
31.105	2.05	Diamyl phthalate	$C_{18}H_{26}O$	306.40
35.122	2.56	Oxiraneoctanoic acid, 3-methyl ester, trans	$C_{19}H_{36}O_3$	312.49
39.111	58.74	Dicarpyl phthalate	$C_{24}H_{38}O_4$	394.59
	100			

Fig. 4.21 GC-MS chromatogram of ethyl alcohol extract of sample NMT03.

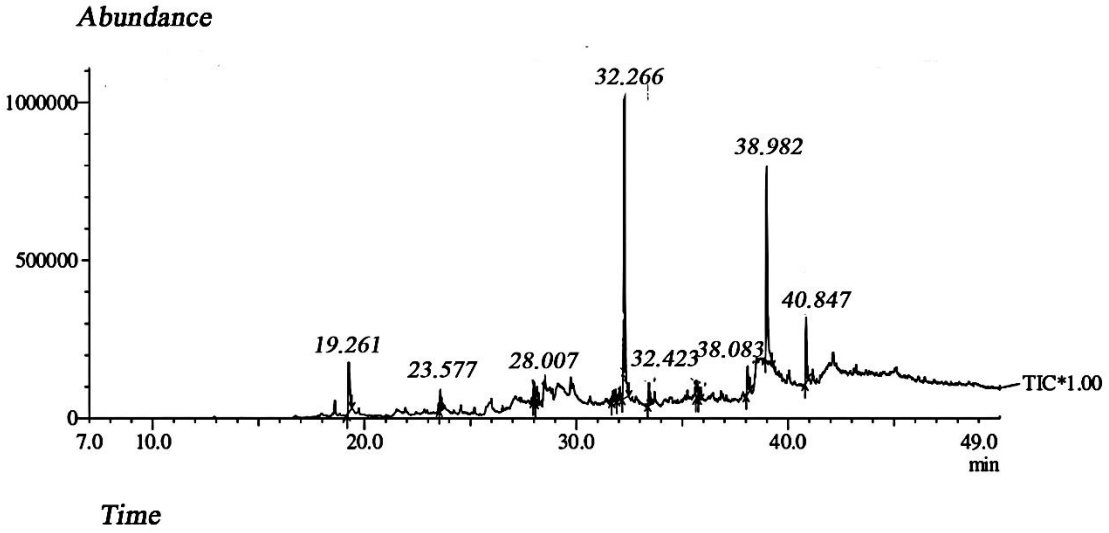

Table 4.12 GC-MS analysis of ethyl alcohol of extract NMT03.

RT(mins)	Peak area %	Name of the compound	Molecular formula	Molecular weight
19.261	7.90	2,4-Ditert-butyl phenol	$C_{14}H_{22}O$	206.32
23.577	1.73	Nonadecane	$C_{19}H_{40}$	268.52
28.007	2.93	2,6,10-trimethyltetradecane	$C_{17}H_{36}$	240.47
28.144	2.81	1-Chlorooctadecane	$C_{18}H_{37}Cl$	288.94
31.728	1.59	2-methyltetracosane	$C_{25}H_{52}$	352.68
32.037	2.08	Tetracosane	$C_{24}H_{50}$	338.65
32.266	38.11	1-Ethylsilatrane	$C_8H_{17}NO_3Si$	203.31
33.423	2.41	1-Eicosanol	$C_{20}H_{42}O$	298.55
35.686	2.36	Tetradecane	$C_{14}H_{30}$	198.39
35.842	1.62	I-Norvaline,N-(2-methoxyethoxycarbonyl)-,pentadecyl ester	$C_{20}H_{39}NO_5$	373.50
38.083	3.74	1,3,5-Trisilacyclohexane	$C_3H_{12}Si_3$	132.38
38.982	25.65	1,2-Benzenedicarboxylic acid	$C_8H_6O_4$	166.13
40.847	7.07	4,4'-((p-Phenylene)diisopropylidene)diphenol	$C_{24}H_{26}O_2$	346.46
	100			

Fig. 4.22 GC-MS chromatogram of ethyl alcohol extract of sample NMT04.

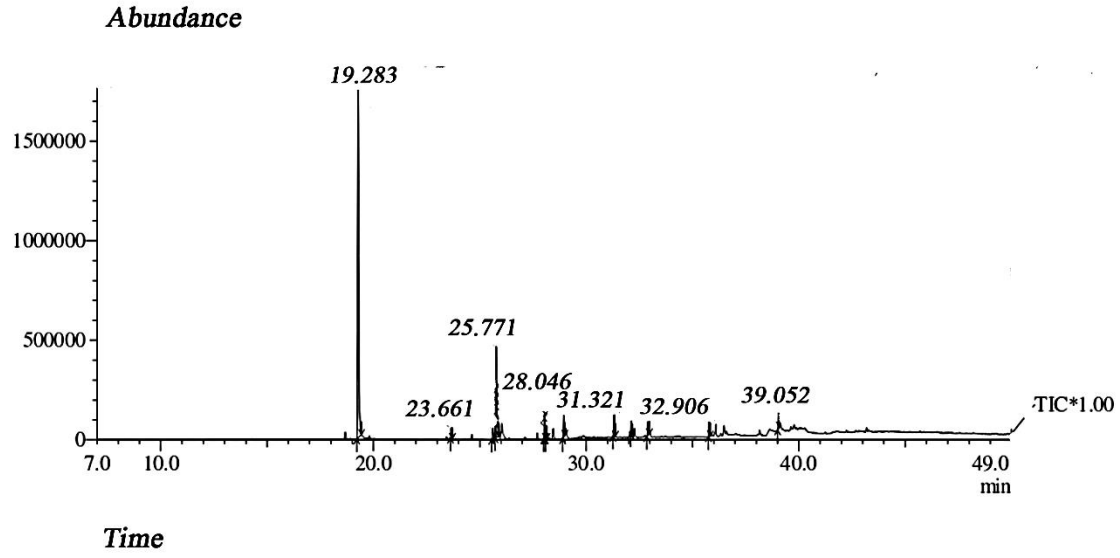

Table 4.13 GC-MS analysis of ethyl alcohol of extract NMT04.

RT(mins)	Peak area %	Name of the compound	Molecular formula	Molecular weight
19.283	62.87	2,4-Ditert-butylphenol	$C_{14}H_{22}O$	206.32
23.661	1.25	Octadecane	$C_{18}H_{38}$	254.49
25.600	1.47	Hexadecanoic acid, methyl ester	$C_{17}H_{34}O_2$	270.45
25.771	14.94	Tetradecanoic acid, 11-methyl-,methyl ester	$C_{16}H_{32}O_2$	256.42
28.046	3.57	7,9-Di-tert-butyl-1-oxaspiro(4,5)deca-6,9-diene-2,8-dione	$C_{17}H_{24}O_3$	276.37
28.117	1.57	Sulfurous acid, hexyl octyl ester	$C_{14}H_{30}O_3Si$	278.45
28.948	2.96	Oxalic acid, 6-ethyloct-3-yl isohexyl ester	$C_{18}H_{34}O_4$	314.46
31.321	3.60	4-Isopropylcyclohexanol	$C_9H_{18}O$	142.24
32.126	1.49	Docosane	$C_{22}H_{46}$	310.60
32.906	2.18	2-Isopropyl-5-methyl-1-heptanol	$C_{11}H_{24}O$	172.31
35.785	1.90	Tridecanol, 2-ethyl-2-methyl-	$C_{16}H_{34}O$	242.44
39.052	2.20	1,2-Benzenedicarboxylic acid, dioctyl ester	$C_{24}H_{38}O_4$	390.56
	100			

Fig. 4.23 GC-MS chromatogram of ethyl alcohol extract of sample NMT06.

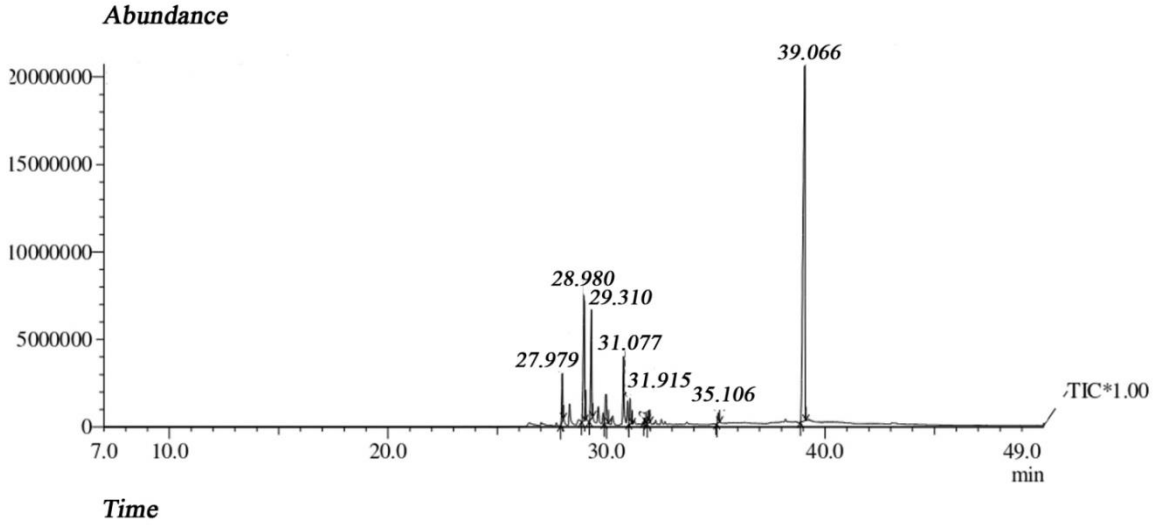

Table 4.14 GC-MS analysis of ethyl alcohol of extract NMT06.

RT(mins)	Peak area %	Name of the compound	Molecular formula	Molecular weight
27.979	4.19	Isobutyl phthalate	$C_{12}H_{13}O_4^-$	221.23
28.980	15.76	Dibutyl phthalate	$C_{16}H_{22}O_4$	278.34
29.310	10.96	Butyl 2-ethylhexyl phthalate	$C_{20}H_{30}O_4$	334.45
29.971	4.07	Phthalic acid, butyl isohexyl ester	$C_{18}H_{26}O$	306.40
31.077	2.17	Diamyl phthalate	$C_{18}H_{26}O_4$	306.40
31.743	0.44	Phthalic acid, 2-methylbutyl pentyl ester	$C_{18}H_{26}O_4$	306.40
31.915	1.17	Di(2-Methoxyethyl) phthalate	$C_{18}H_{26}O_4$	306.40
35.106	0.95	Methyl cis-9,10-epoxyoctadecanoate	$C_{19}H_{36}O_3$	312.49
39.066	60.33	1,2-Benzenedicarboxylic acid	$C_8H_6O_4$	166.13
	100			

Fig. 4.24 GC-MS chromatogram of ethyl alcohol extract of sample NMT07

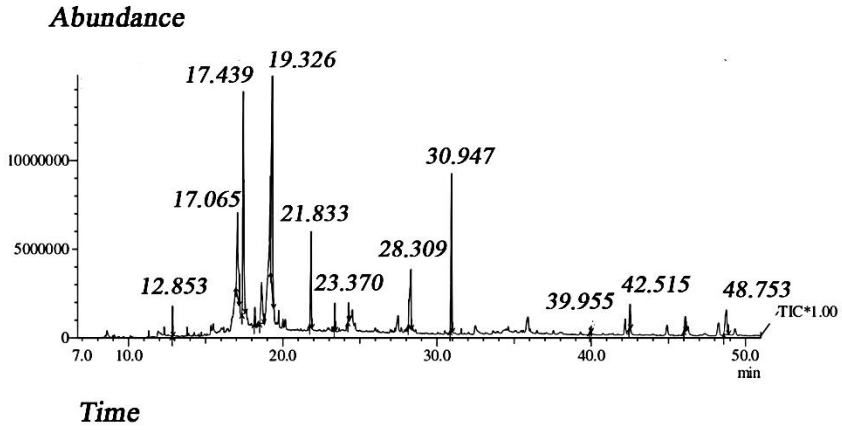

Table 4.15 GC-MS analysis of ethyl alcohol of extract NMT07.

RT(mins)	Peak area %	Name of the compound	Molecular formula	Molecular weight
12.853	1.12	2,4 Di-tert-butylphenol	$C_{14}H_{22}O$	206.32
17.065	9.40	9-Octadecenoic acid	$C_{18}H_{34}O_2$	282.46
17.439	20.10	Phthalic acid, butyl undecyl ester	$C_{23}H_{36}O_4$	376.53
18.190	1.34	Acetamide, 2-(Diethylamino)-N-(2,6-Dimethylphenyl)	$C_{12}H_{18}N_2O$	234.34
18.634	5.90	Cyclo(leucylopropyl)	$C_{11}H_{18}N_2O_2$	210.27
19.326	24.57	Dibutyl Phthalate	$C_{16}H_{22}O_4$	278.34
21.833	6.82	n-Nonadecanol-1	$C_{19}H_{40}O$	284.52
23.370	1.52	Bis(2-ethylhexyl)maleate	$C_{20}H_{36}O_4$	338.48
24.265	1.04	Eicosane	$C_{20}H_{42}$	282.55
28.309	7.99	Pyrrolo(1,2-a)pyrazine-1,4-dione,hexahydro-3-(phenylmethyl)	$C_7H_{10}N_2O_2$	244.29
30.947	11.96	1,2-benzenedicarboxylic acid	$C_8H_6O_4$	166.13
39.955	0.39	Myristyl myristate	$C_{28}H_{56}O_2$	424.74
42.515	2.00	Docosyl pentafluoropropionate	$C_{25}H_{45}F_50_2$	472.62
46.103	1.62	Hexadecanoic acid, Hexadecyl ester	$C_{32}H_{64}O_2$	480.85
48.753	4.23	Tetracosyl heptafluorobutyrate	$C_{28}H_{49}F_7O_2$	550.68
	100			

Fig. 4.25 GC-MS chromatogram of ethyl alcohol extract of sample NMT08.

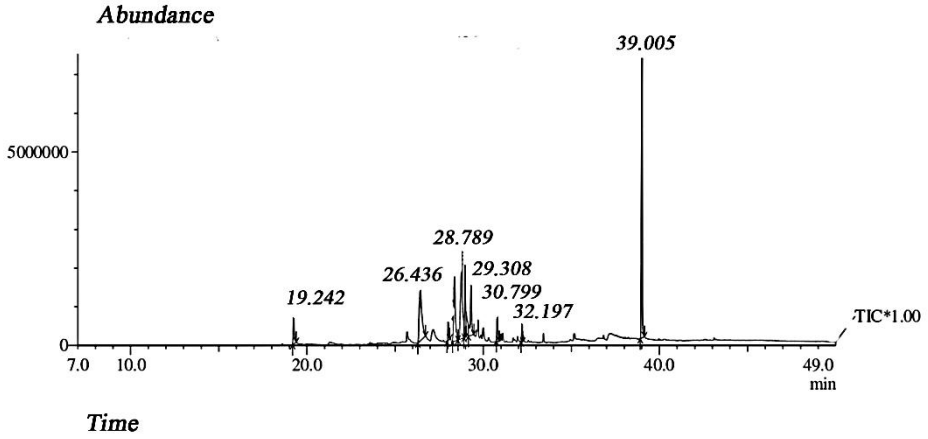

Table 4.16 GC-MS analysis of ethyl alcohol of extract NMT08.

RT(mins)	Peak area %	Name of the compound	Molecular formula	Molecular weight
19.242	3.82	Phenol,2,4-bis(1,1-dimethylethyl)-	$C_{14}H_{22}O$	206.32
26.436	15.49	3-Isobutylhexahydropyrrolo(1,2-A)pyrazine-1,4-dione	$C_{11}H_{18}N_2O_2$	210.27
28.009	1.83	Isobutyl phthalate	$C_{12}H_{13}O_4$	221.23
28.366	12.24	Cyclo(leucyloprolyl)	$C_{11}H_{18}N_2O_2$	210.27
28.789	19.20	Cyclo-L-prolyl-L-leucine	$C_{11}H_{18}N_2O_2$	210.27
28.970	8.88	Dibutyl phthalate	$C_{16}H_{22}O_4$	278.34
29.308	7.14	Butyl isobutyl phthalate	$C_{16}H_{22}O_4$	278.34
30.799	2.64	Bismethylglycol	$C_4H_{10}O_2$	90.12
32.197	1.60	Octadecanoic acid, methyl ester	$C_{19}H_{38}O_2$	298.50
39.005	27.14	1,2-Benzenedicarboxylic acid	$C_8H_6O_4$	166.13
	100			

Fig. 4.26 GC-MS chromatogram of ethyl alcohol extract of sample NMT09.

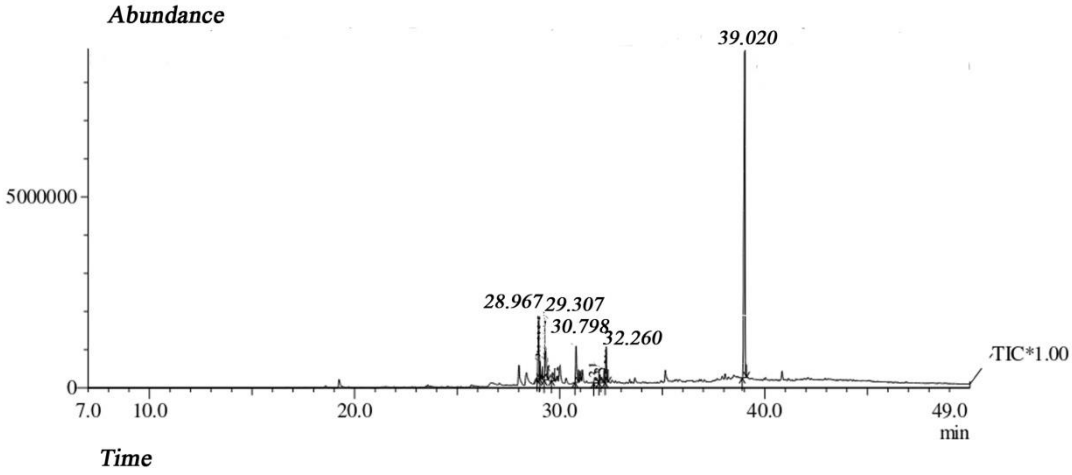

Table 4.17 GC-MS analysis of ethyl alcohol of extract NMT09.

RT(mins)	Peak area %	Name of the compound	Molecular formula	Molecular Weight
28.967	11.28	Dibutyl phthalate	$C_{16}H_{22}O_4$	278.34
29.033	2.20	Di(2-ethylhexyl) phthalate	$C_{24}H_{38}O_4$	390.56
29.307	9.71	Butyl 2-ethylhexyl phthalate	$C_{20}H_{30}O_4$	334.45
29.653	2.23	Diamyl phthalate	$C_{18}H_{26}O_4$	306.40
30.798	6.36	Octyl butyl phthalate	$C_{20}H_{30}O_4$	334.45
31.692	1.96	Methyl (7E)-7-hexadecenoate	$C_{17}H_{32}O_2$	268.43
31.950	2.02	1,2-Benzenedicarboxylic acid, butyl 2-ethylhexyl ester	$C_{20}H_{30}O_4$	334.45
32.260	5.35	1-allyl-2,8,9-trioxa-5-aza-1-silabicyclo(3.3.3)undecane	$C_9H_{17}NO_3Si$	215.32
39.020	58.89	1,2-Benzenedicarboxylic acid	$C_8H_6O_4$	166.13
	100			

4.4 Total phenolic content of sample isolates

The total phenol content of the ethyl alcohol extract of the samples was calibrated with standard gallic acid and also the percentage of yield was tabulated (Table 4.18). Thus, out of eight samples, *Bacillus vietnamensis* SMC (NMT07) contains more phenolic content with estimated value of 226.04 ±0.04 µg/mg of the extract calculated as Gallic Acid Equivalent (GAE). Also, the percentage of yield of NMT07 was found to be calculated as 22.6% (Fig. 4.27).

Fig. 4.27 TPC of sample extract (a) and calibration curve of standard Gallic acid (b).

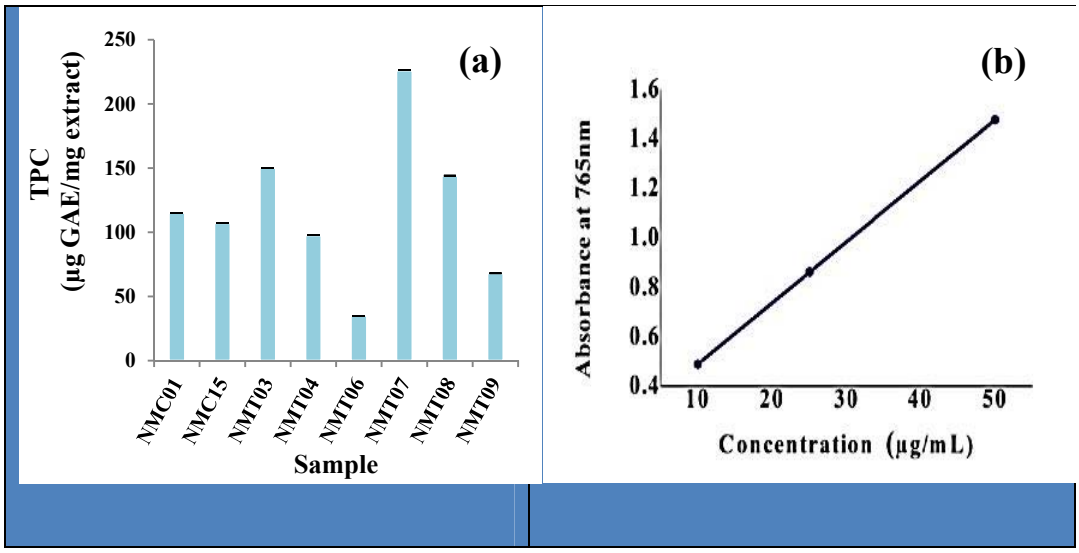

Table 4.18 Total phenolic content and percentage yield of sample extract.

Sample	TPC (µg GAE/mg extract)	% yield
NMC01	115.08 ±0.02	11.50%
NMC15	107.08 ±0.01	10.7%
NMT03	150.12 ±0.01	15.01%
NMT04	97.62 ±0.02	9.76%
NMT06	35.04 ±0.01	3.5%
NMT07	226.04 ±0.04	22.6%
NMT08	144.08 ±0.02	14.4%
NMT09	68.16 ±0.03	6.8%

4.5 Biogenic iron oxide nanoparticle synthesis

On exposure of culture supernatant of selected eight endophytic isolates to $FeCl_3$ solution, the reaction mixture of *Exiguobacterium aurantiacum* NMC1 (NMC01) showed an appreciable color change from pale yellow to dark brown (Fig. 4.28), indicating the formation of iron oxide nanoparticles.

Fig. 4.28 Photograph of visual observation of synthesized iron oxide nanoparticles

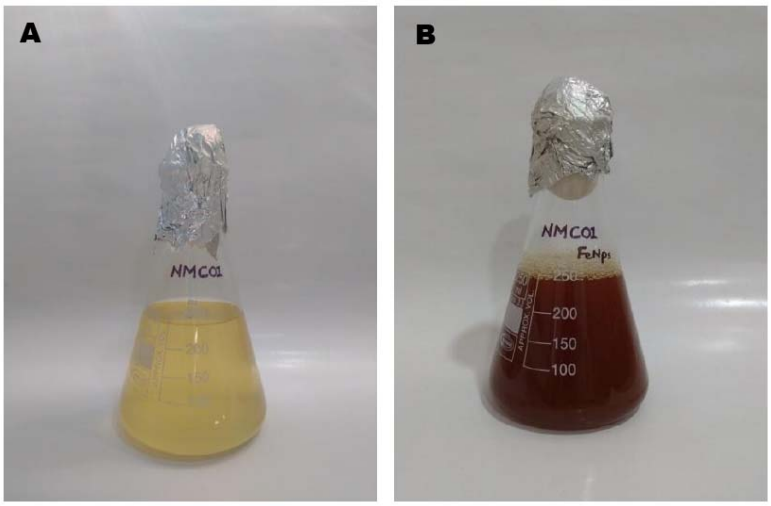

A-Culture supernatant of *Exiguobacterium aurantiacum* NMC1.

B-Culture supernatant with $FeCl_3$ solution (color changes from pale yellow to brown).

The bacterially synthesized iron oxide NPs was characterized by UV-Vis spectroscopy, FTIR, EDAX, SEM, XRD and TEM. The observed color change was further confirmed by UV-Vis spectral analysis, which showed an intense absorption peak due to surface Plasmon excitation at 293.50 nm, indicating iron oxide NPs. The FTIR analysis showed functional groups –OH stretching, –OH with hydrogen bonding, C-H stretching, –NH bending, alkane groups, and P-O stretching corresponding to the peak 3421.72 cm^{-1}, 3742.72 cm^{-1}, 2362.80 cm^{-1}, 1627.92 cm^{-1}, (1546.91 and 1519.91 cm^{-1}), and 1022.27 cm^{-1}, respectively. In contrast, the peaks 669.30 and 524.64 cm^{-1} lies in the fingerprint region (Nakamoto, 1997). These functional groups represents bacteria-derived exometabolites are capped with iron oxide nanoparticles.

Fig. 4.29 UV-Vis absorption spectrum of iron oxide nanoparticles of NMC01.

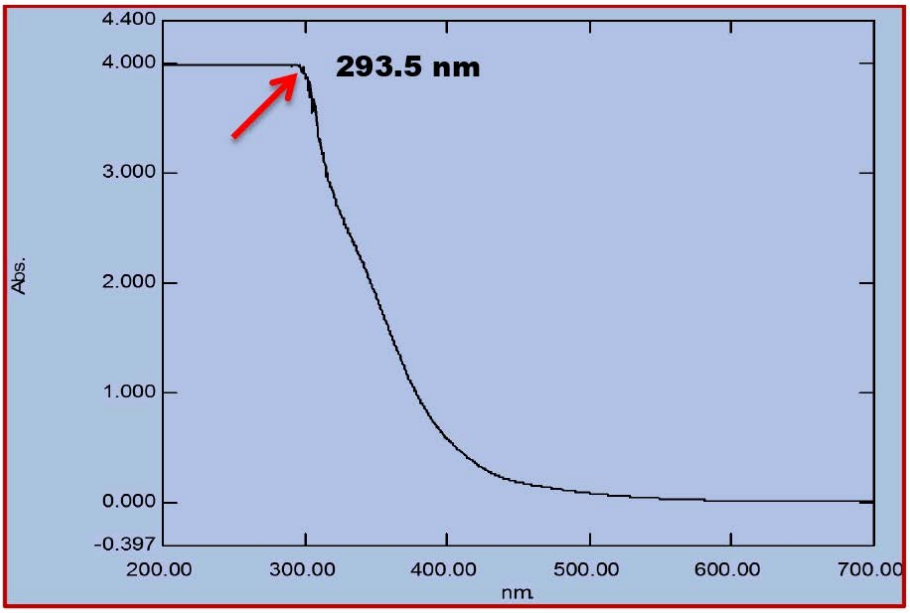

Fig. 4.30 FTIR analysis of iron oxide nanoparticles of NMC01.

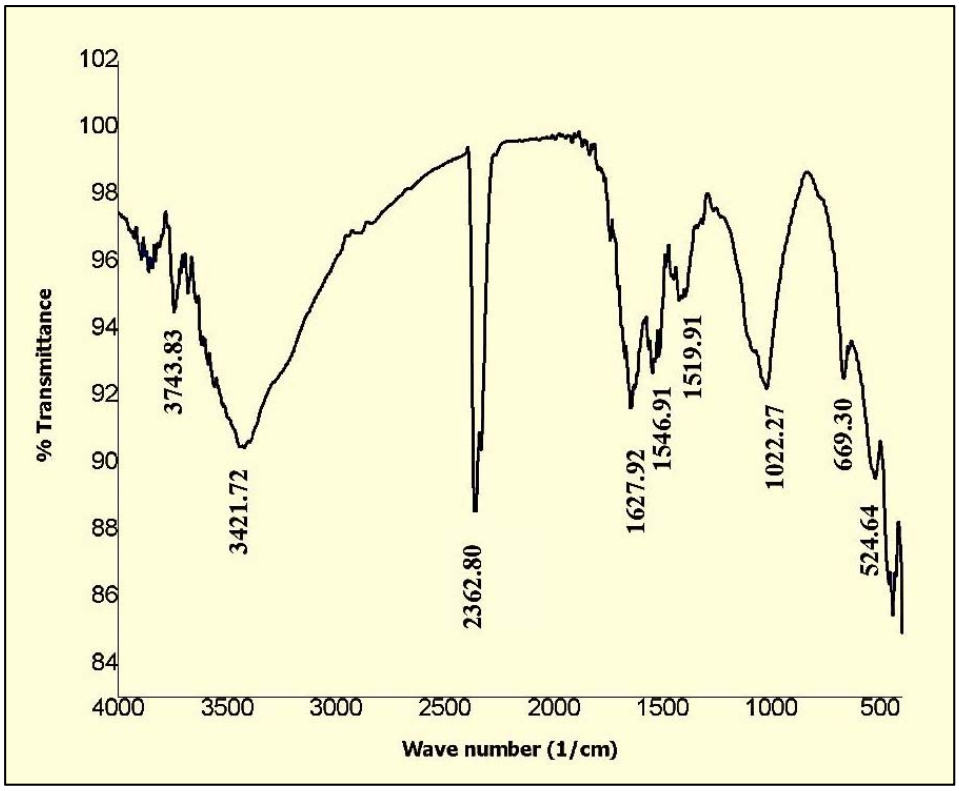

EDAX analysis of synthesized γ-Fe_2O_3 nanoparticle (Fig. 4.31) indicates the presence of Fe metal and Oxygen elements in the sample, indicating the purity of synthesized nanoparticles.

Fig. 4.31 EDAX image of iron oxide nanoparticles of NMC01.

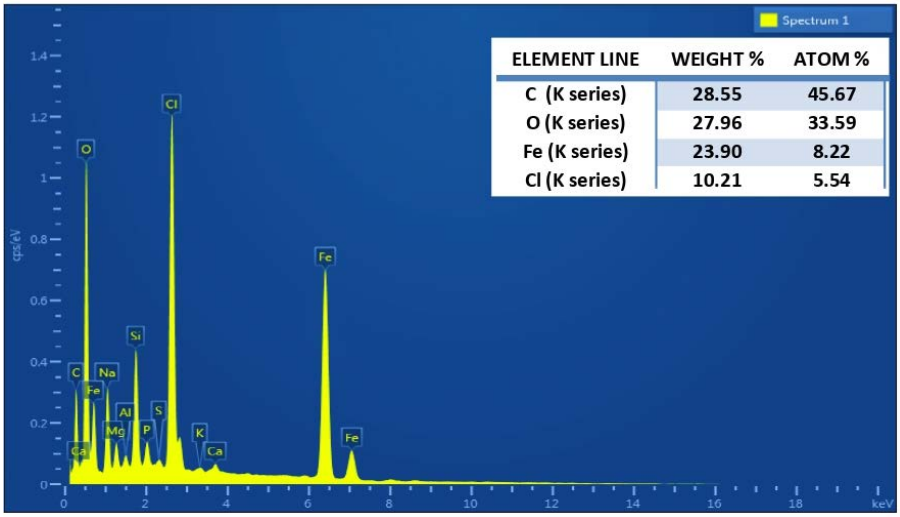

Scanning Electron Microscopy images (Fig. 4.32) show that the particles are in the Nano region and spherical, along with some aggregation of nanoparticles.

Fig. 4.32 SEM image of iron oxide nanoparticles of NMC01.

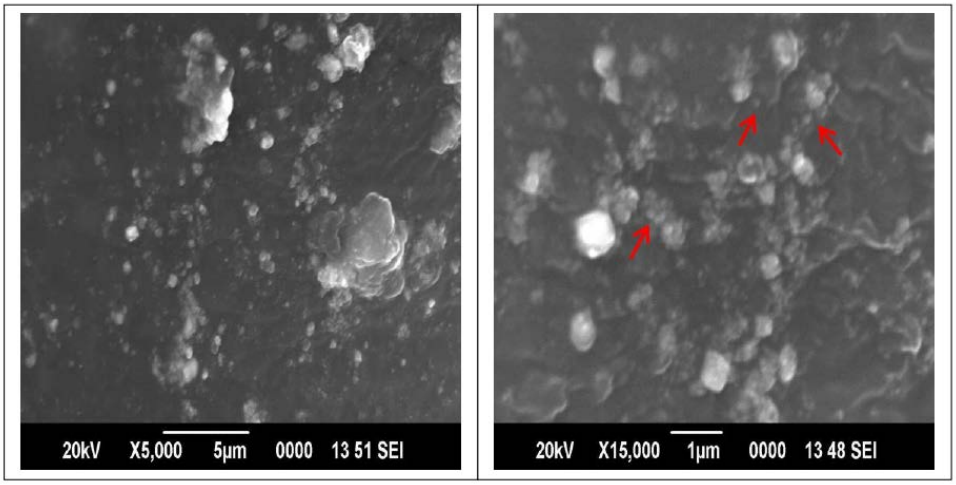

Fig. 4.33 shows an X-ray diffraction pattern carrying out phase identification. XRD indicates the (220), (311), (400), (422), (511), and (440) planes observed at peak 27.8, 32.0, 45.0, 54.0, 56.7 and 66.6 º, confirms γ-Fe_2O_3 by comparing with Joint Committee on Powder Diffraction Standards (JCPDS cards no. 39-1346). Furthermore, using Debye-Scherrer's formula, the mean average crystalline size calculated for the most intense peak (311) was 42.98 nm. TEM analysis showed the particle's size range with a diameter between 9.05 nm and 51.21 nm (Fig. 4.34).

Fig. 4.33 X-Ray Diffraction curves of iron oxide nanoparticles of NMC01.

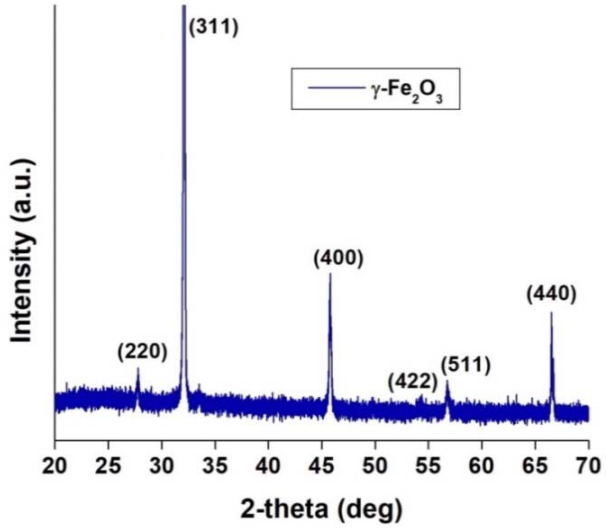

Table 4.19 X- ray diffraction data (2θ and d-spacing of nanocrystal peak).

2θ (º)	**Peal planes**	**D-spacing (nm)**
27.8	(220)	3.85
32.0	(311)	2.80
45.0	(400)	2.01
54.0	(422)	1.69
56.7	(511)	1.62
66.6	(440)	1.41

Fig. 4.34 TEM micrograph (A) with SAED pattern (B) of iron oxide nanoparticles of NMC01.

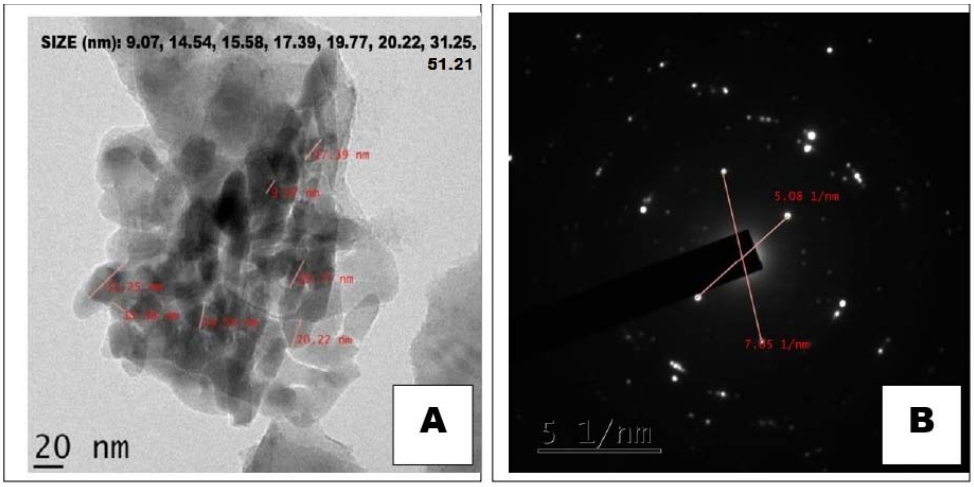

4.5.1 Heavy metal removal and dye decoloration

Heavy metal removal study by synthesized γ-Fe_2O_3 (maghemite) nanoparticle using AAS method showed significant result. Removal efficiencies of Pb(II), Cd(II) and Cr(III) by synthesized nanoparticle was shown in table 4.20 and fig. 4.35. The test concentration of lead, cadmium and chromium was found to be low in treated water when compared to control.

Table 4.20 Heavy metals removal by synthesized γ-Fe_2O_3 nanoparticle.

Heavy metal	Control Conc. (mg/L)	Test Conc. (mg/L)
Lead (Pb)	0.94	-
Cadmium (Cd)	0.922	0.37
Chromium (Cr)	1.0	0.712

Fig. 4.35 Graph showing heavy metals removal from treated water using AAS.

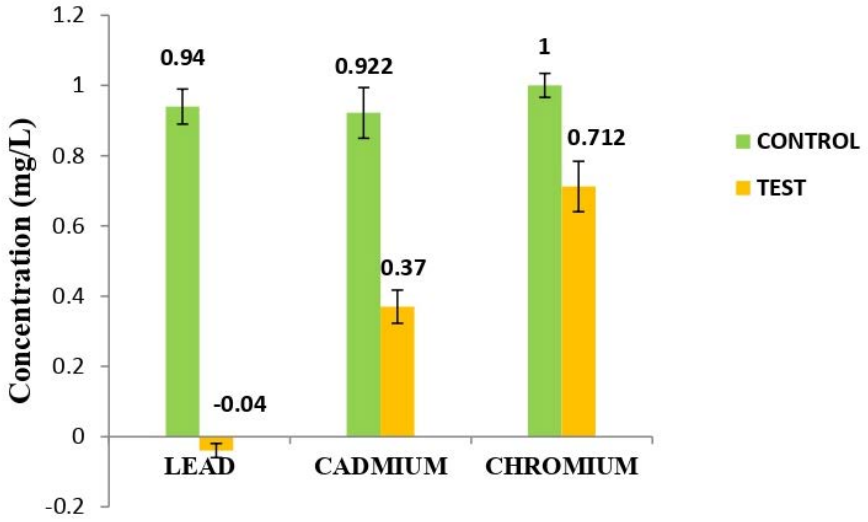

Azo dyes such as Eriochrome Black T, Congo red, and Trypan blue, were selected for the dye decoloration test of synthesized γ-Fe_2O_3 nanoparticle. The results show the maximum percentage of dye decoloration in Congo red (88.2%), followed by Trypan blue (63.69%) and Eriochrome Black T (50%) as shown in table 4.21 and fig. 4.36.

Table 4.21 Degradation of different dye by synthesized γ-Fe_2O_3 nanoparticle

Dye	**Max. abs. wavelength (nm)**	**Control (OD)**	**Test (OD)**	**% of dye degradation**
Eriochrome Black T	545	0.131	0.065	50%
Congo red	497	0.589	0.069	88.28%
Trypan blue	540	0.942	0.342	63.69%

Fig. 4.36 Photograph of dye decoloration by synthesized γ-Fe_2O_3 nanoparticle.

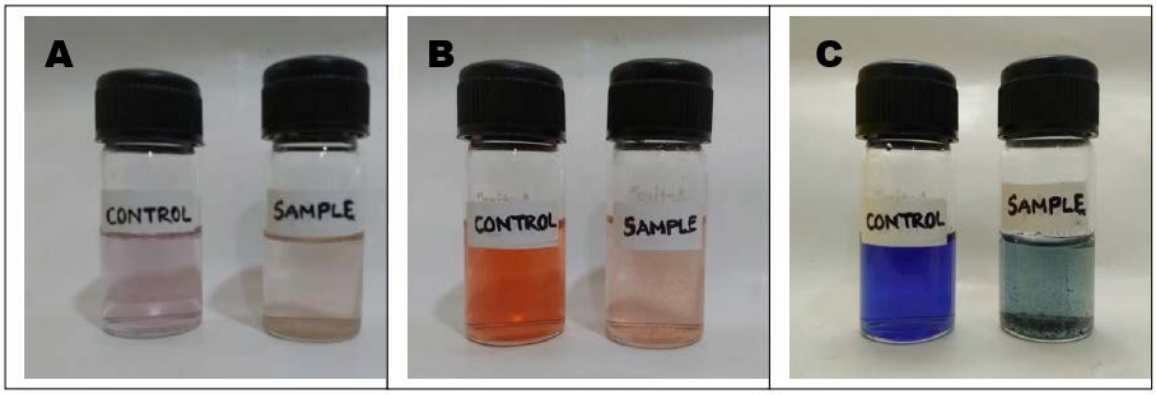

A= Eriochrome Black T, **B**= Congo Red, **C**=Trypan Blue

4.6 Antimicrobial screening of selected isolates

4.6.1 Antibacterial activity

Eight isolates were screened for antibacterial activity against five human pathogens using the cross-streak method; out of it *Exiguobacterium aurantiacum* NMC1 only showed antagonistic activity against *Escherichia coli*, *Listeria* sp., *Klebsiella* sp., and *Streptococcus* sp. when compared to the control plate. Also, no inhibition on the growth of *Shigella* sp. was recorded.

Fig. 4.37 Plates showing antibacterial activity of *Exiguobacterium aurantiacum* NMC1 by cross-streak method.

4.6.2 Antifungal activity

The antifungal activity of the selected isolates was estimated using dual plate culture method. The plant pathogens *Sclerotium rolfsii* and *Aspergillus* sp. were selected for the antifungal study of the isolates. The sample NMT03 and NMT04 showed significant fungal growth inhibition in both the pathogens. NMT06 isolate showed maximum inhibition on the growth of *Aspergillus* sp. at 52.96% and found no inhibition on *Sclerotium rolfsii* growth, whereas NMT04 isolate showed maximum inhibition on *Sclerotium rolfsii* at 47.04% (Table 4.22). Furthermore, another isolate, NMT09 showed 45.55% inhibition on *Sclerotium rolfsii* growth and found no inhibition on *Aspergillus* sp. (Fig. 4.38 and Fig. 4.39).

Table 4.22 Percentage of fungal growth inhibition by isolated bacteria.

Sample	Percentage of fungal growth inhibition	
	Sclerotium rolfsii	***Aspergillus* sp.**
NMT03	29.26%	35.93%
NMT04	47.04%	42.96%
NMT06	-	52.96%
NMT09	45.55%	-
CONTROL	-	-

Fig. 4.38 Plates showing antifungal activity of isolates against phytopathogen *Sclerotium rolfsii* by dual culture method.

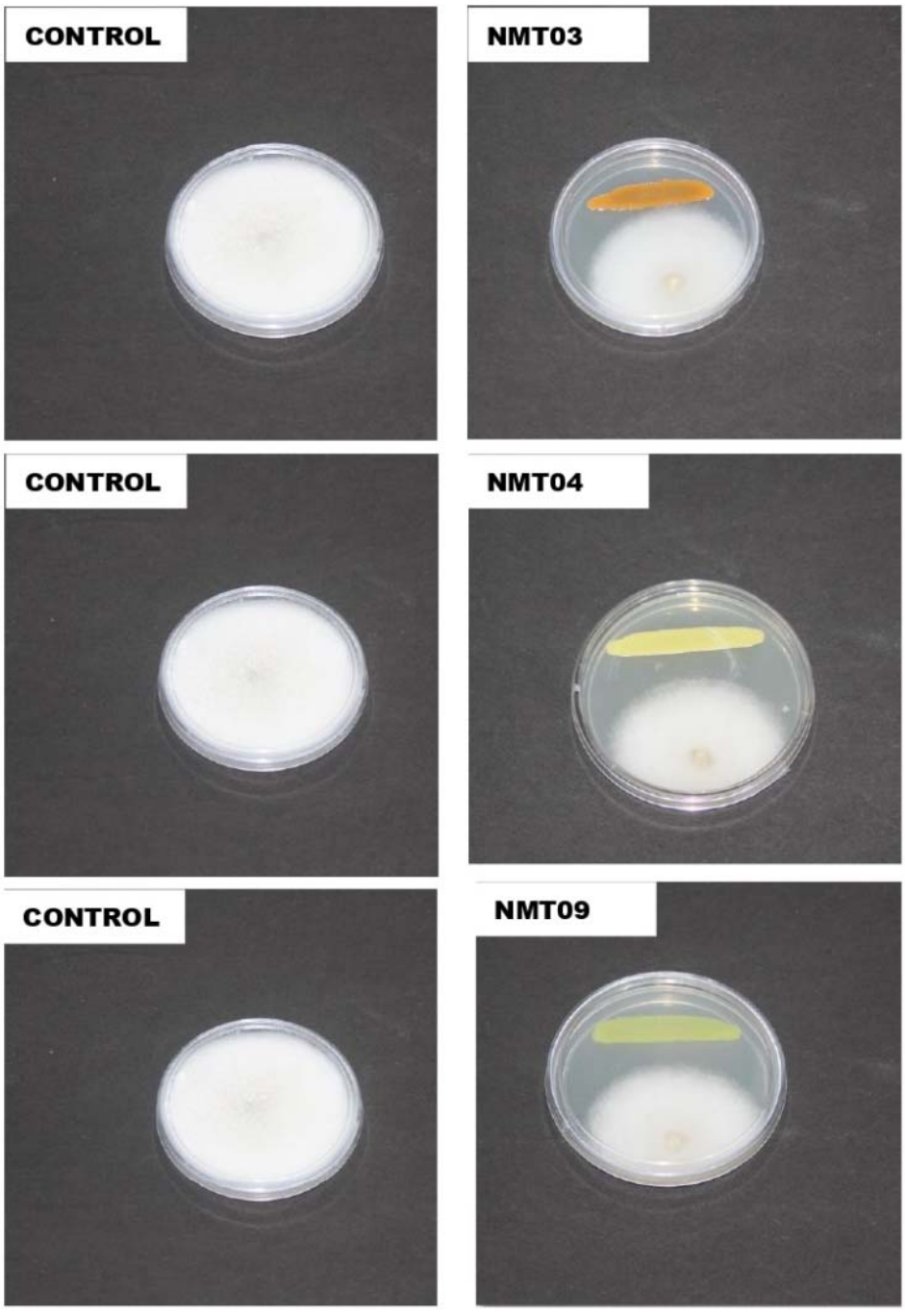

Fig. 4.39 Plates showing antifungal activity of isolates against phytopathogen. *Aspergillus* sp. by dual culture method.

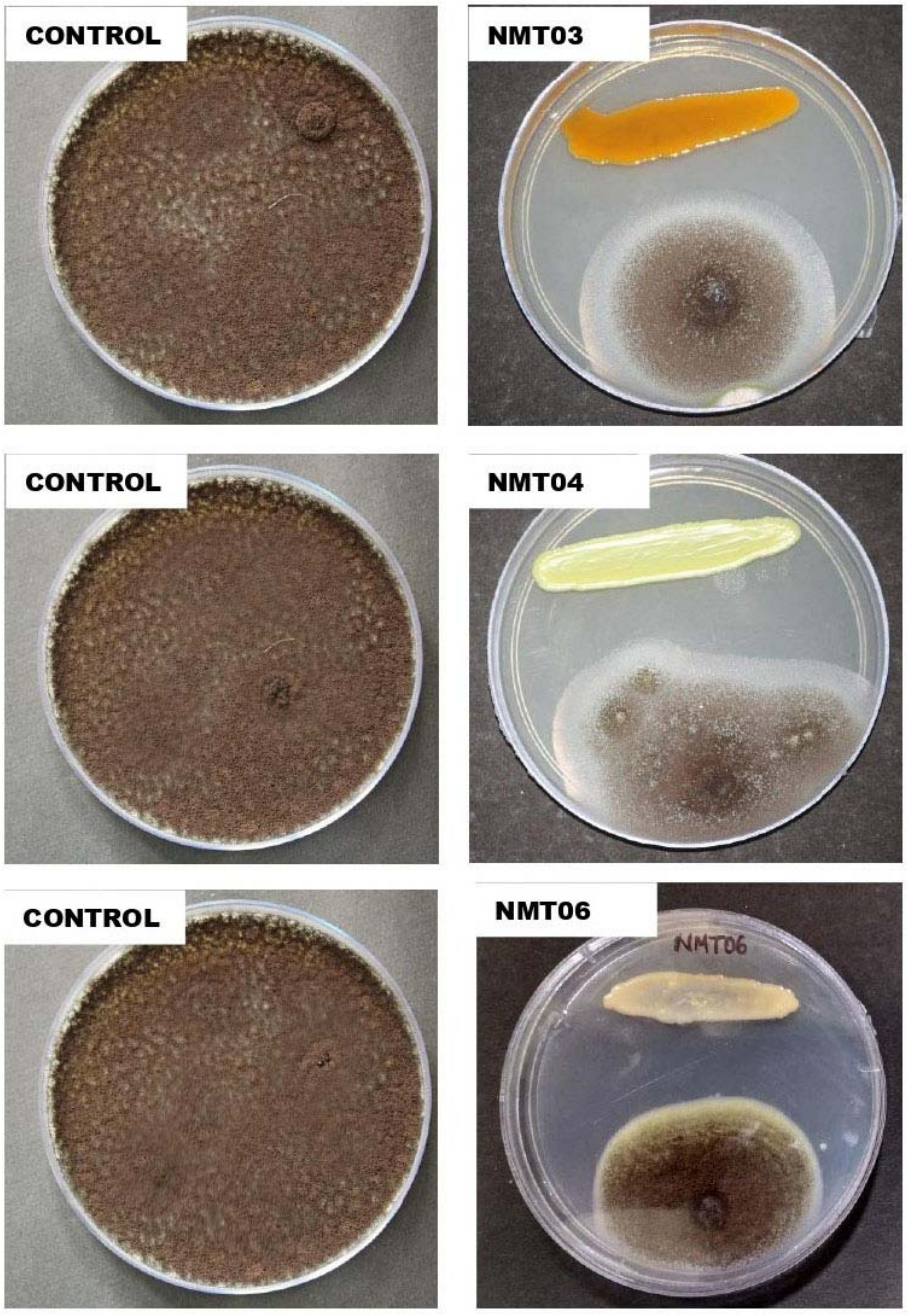

4.7 In vitro antioxidant assay

4.7.1 DPPH assay

In this assay, DPPH solution got discolored, pointing towards the radical scavenging property of the isolates. The samples extract were found to scavenge efficiently in a concentration-dependent manner. Among eight samples, NMT03 effectively scavenge DPPH free radical with an IC_{50} value of 49.13 ±0.76 µg/mL (Fig 4.40 and 4.41).

Fig. 4.40 DPPH radical scavenging activity of ethyl alcohol extract of samples.

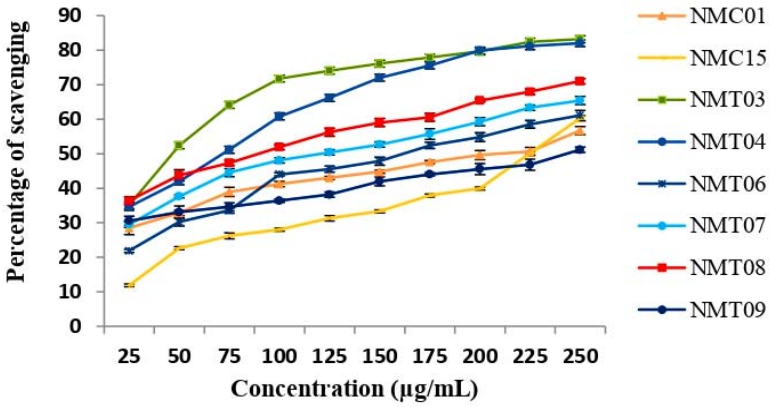

Fig. 4.41 IC $_{50}$ value of the sample extract in DPPH assay.

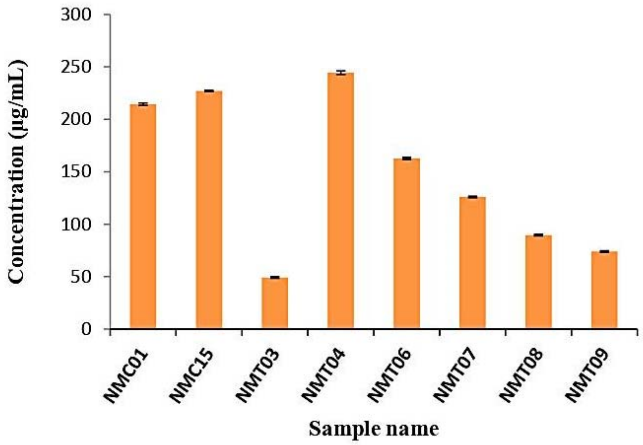

4.7.2 Superoxide radical scavenging (SRSA) assay

The ethyl alcohol extract of the isolates was found to scavenge superoxide radicals significantly (Fig. 4.42). Among all the samples, NMT06 extract shows effective scavenging with an IC_{50} value of 63.71 ±0.84 µg/mL (Fig. 4.43). On the other hand, the standard drug (ascorbic acid) has an IC_{50} value of 23.02 ±1.02 µg/mL.

Fig. 4.42 SRSA activity of ethyl alcohol extract of samples

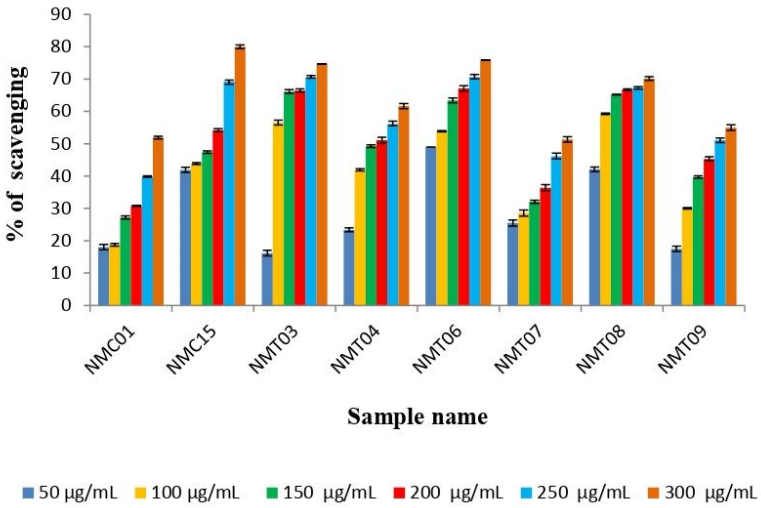

Fig. 4.43 IC_{50} value of the sample extract in SRSA assay.

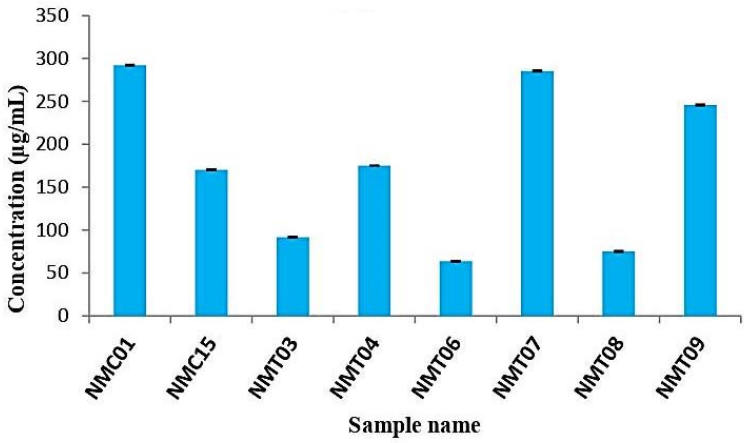

4.7.3 Lipid peroxidation inhibition (LPI) assay

Lipid peroxidation inhibition activity of the isolates extract was carried out in rat liver homogenate. All the samples taken for the study labelled significant inhibition of lipid peroxidation except the sample NMC15. NMT06 performed the highest inhibition activity with an IC_{50} value of 27.3 ±0.65 µg/mL when compared to standard drug (BHT) with an IC_{50} value of 15.4 ±1.59 µg/mL.

Fig. 4.44 LPI activity of ethyl alcohol extract of samples.

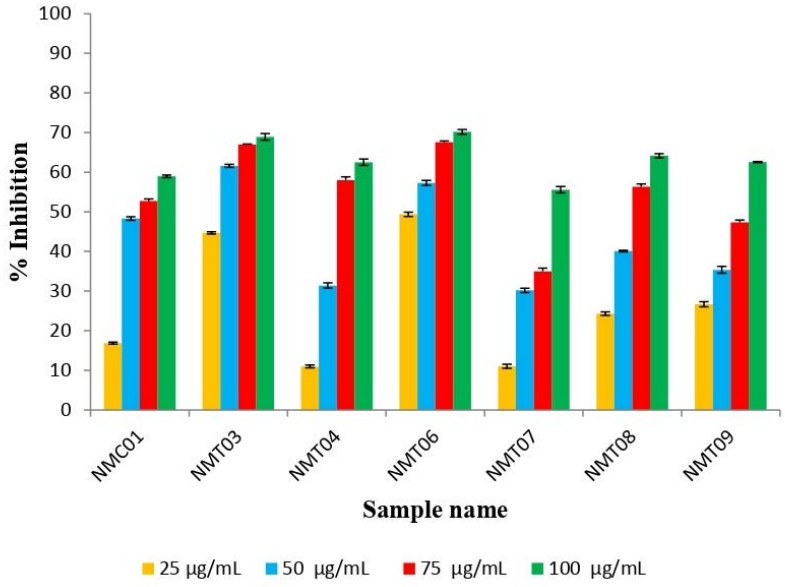

Fig. 4.45 IC_{50} value of the sample extract in LP1 assay.

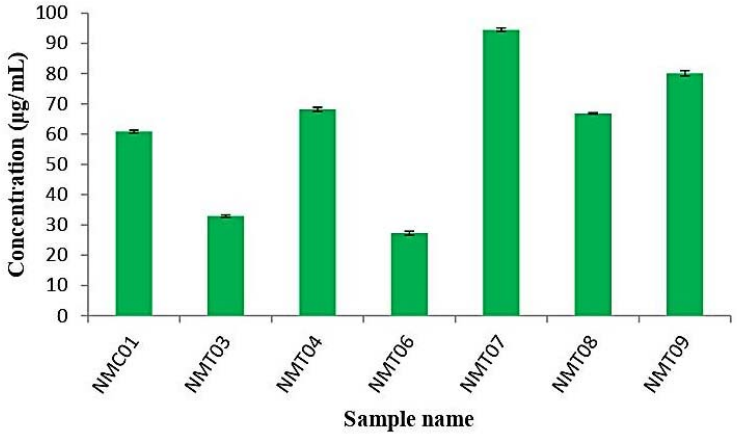

4.7.4 Ferric Reducing Antioxidant Power (FRAP) assay

In the FRAP assay, the yellow color of the solution changes to various shades of green based on the reducing power of each compound. All the samples exhibited this assay has reducing potential, and absorbance was recorded (Fig. 4.46). The sample NMT07 has maximum reducing power with an IC_{50} value of 33.55 ±0.69 µg/mL (Fig. 4.47), when compared with ascorbic acid (standard) having an IC_{50} value of 4.45 ±1.27 µg/mL.

Fig. 4.46 FRAP of ethyl alcohol extract of samples.

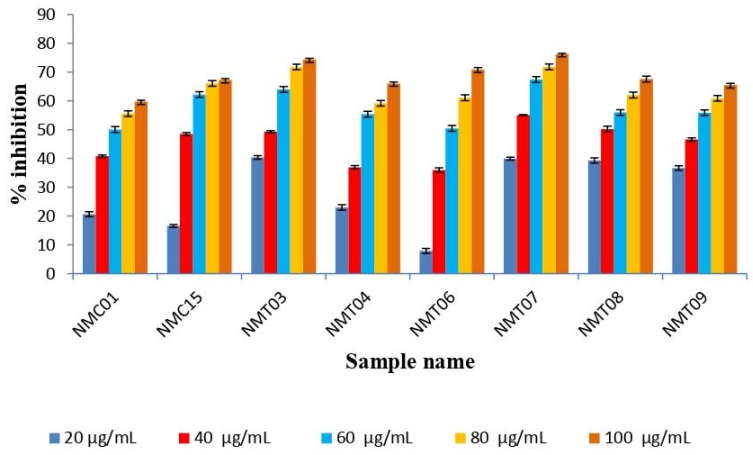

Fig. 4.47 IC_{50} value of the sample extract in FRAP assay.

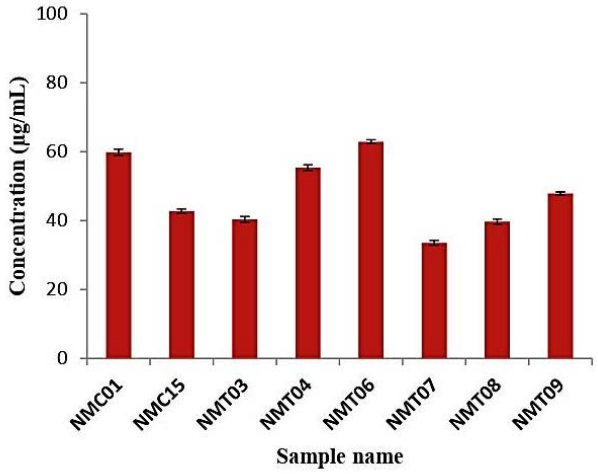

The IC_{50} value of all the sample extract when compared with reference standard has been shown in table 4.23. The data represents the isolates difference in antioxidant activity with the varied concentration to achieve the IC_{50} value.

Table 4.23 The IC_{50} value of samples and standard drug of different antioxidant assay.

Sample	IC_{50} value (µg/mL)			
	DPPH	**SRSA**	**LPI**	**FRAP**
NMC01	214.27 ±1.16	292.24 ±0.41	60.89 ±0.57	59.82 ±0.88
NMC15	227.13 ±0.45	170.26 ±0.36	-	42.76 ±0.64
NMT03	49.13 ±0.76	91.77 ±0.77	32.96 ±0.37	40.38 ±1.11
NMT04	244.42 ±1.59	175.36 ±0.90	68.18 ±0.66	55.37 ±0.80
NMT06	162.64 ±0.93	63.71 ±0.84	27.3 ±0.65	62.87 ±0.54
NMT07	126.06 ±0.76	285.35 ±0.94	94.4 ±0.55	33.55 ±0.69
NMT08	89.54 ±0.76	75.16 ±0.50	66.86 ±0.67	39.69 ±0.62
NMT09	74.13 ±0.76	245.84 ±0.87	80.15 ±0.87	47.86 ±0.59
Ascorbic acid (standard)	19.02 ±1.11	23.02 ±1.02	-	4.45 ±1.27
BHT (standard)	-	-	15.4 ±1.59	-

4.8 In vitro cytotoxicity study

4.8.1 Short term in vitro cytotoxicity study

The ethyl alcohol extract of the selected eight bacterial samples shows cytotoxicity toward DLA cells, as observed from the short-term trypan blue exclusion method. In addition, a dose-dependent increase in cytotoxicity of the extract was noted. Among eight samples, NMC15 and NMT07 show IC_{50} values below 50 µg/mL, as shown in table 4.24 and fig. 4.48. So, these two samples were selected for in vivo studies.

Table 4.24 The IC_{50} value of sample extract on cytotoxicity towards DLA cell lines.

Sample	IC_{50} (µg/mL) ± SEM*
NMC01	133.62 ±0.848
NMC15	47.51 ±0.183
NMT03	148.98 ±0.141
NMT04	78.23 ±0.353
NMT06	150.70 ±0.876
NMT07	44.12 ±0.311
NMT08	62.87 ±0.480
NMT09	125.10 ±0.353

*SEM- Standard error of mean

Fig. 4.48 In vitro cytotoxicity analysis of 8 samples extract towards DLA cell lines

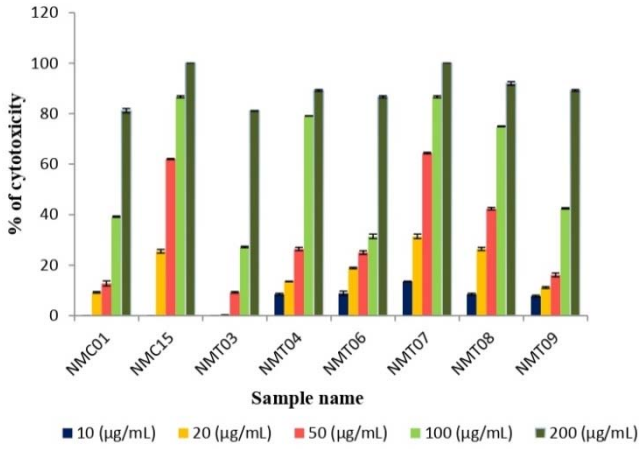

4.8.2 MTT assay

The effect of sample NMC15 and NMT07 extracts on the viability of cancer cells was determined by MTT assay on MCF-7 cell lines. The predicted IC_{50} value for NMC15 and NMT07 were 79.36 ±1.91 µg/mL and 98.91 ±1.86 µg/mL, respectively.

Fig. 4.49 Cell viability profile of NMC15 extract against MCF-7 breast cancer cell lines.

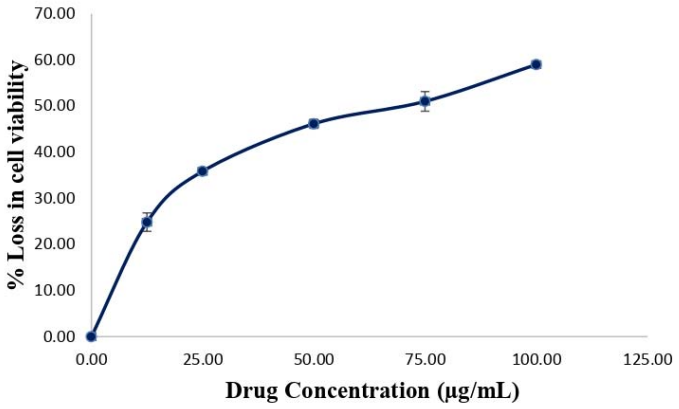

Fig. 4.50 Cell viability profile of NMT07 extract against MCF-7 breast cancer cell lines.

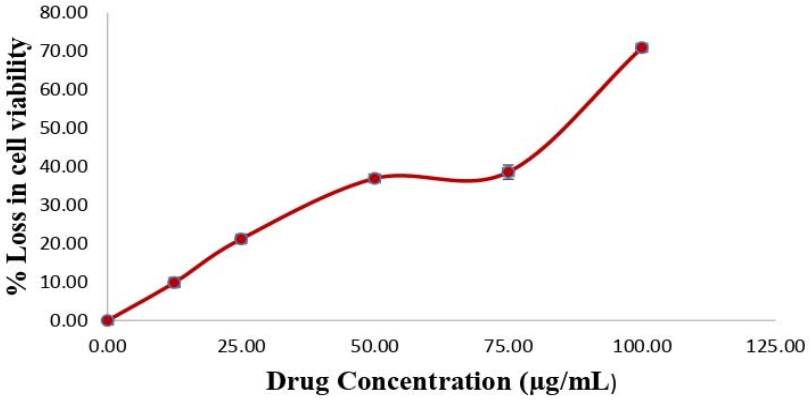

4.9 In vivo study

4.9.1 Toxicity study

The administration of propylene glycol extract of the samples (NMC15 and NMT07) of a single dose (300 mg/kg b.wt.) in mice reported no observable toxicity such as weight loss, hair loss, skin color change, food, and water intake difference. Also, no mortality was recorded, assuming the drug is safe for in vivo studies.

4.9.2 Anti-inflammatory study

The sample extracts NMC15, and NMT07 screened after in-vitro and in vivo toxicity analysis were used to study acute and chronic anti-inflammatory activity in male Swiss albino mice. The paw edema is induced by carrageenan (acute) and formalin (chronic), were significantly reduced on treating the mice with sample extract when compared with the control mice.

Fig. 4.51 Inflammation-induced in mice [A] before induction and [B] after induction.

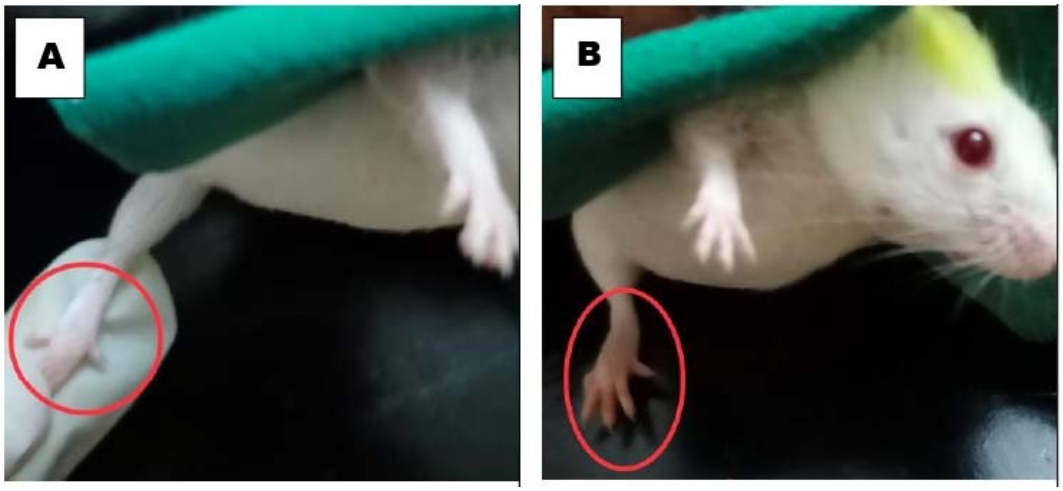

4.9.2.1 Inhibition of carrageenan-induced inflammation

Acute anti-inflammatory activity of ethyl alcohol extract of *Brevundimonas vesicularis* JAP (NMC15) and *Bacillus Vietnamensis* SMC (NMT07) was

determined. Carrageenan was used as an inflammatory agent in mice. When compared with the control, extract-treated animals showed a significant reduction in carrageenan-induced paw edema. The sample extracts NMC15 at 25, and 50 mg/kg doses exhibited activity with 32.71 and 34.57 % inhibition at the 3rd hour, respectively (Fig. 4.52 and Table 4.25). The anti-inflammatory effect of the NMT07 sample was effective in reducing acute inflammation induced by carrageenan with percentage inhibition of 17.75 and 37 % at the 3rd hour for the doses of 25 and 50 mg/kg, respectively. Administration of standard anti-inflammatory agent diclofenac also reduced carrageenan-induced inflammation with 45.79% inhibition (Fig. 4.53 and Table 4.26).

Fig. 4.52 Effect of sample NMC15 on carrageenan- induced acute inflammation in reducing the paw edema in Swiss albino mice.

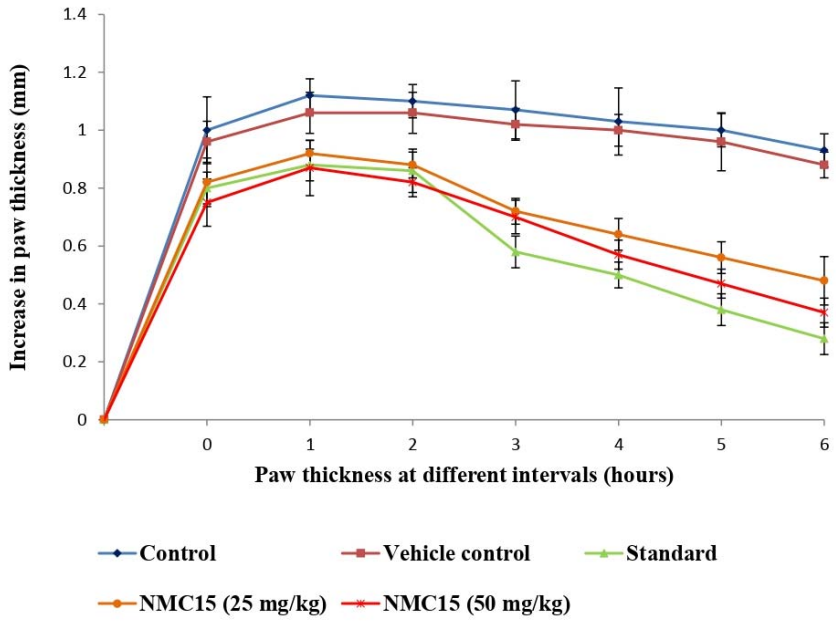

Table 4.25 Inhibition of carrageenan-induced acute inflammation by NMC15 extract.

GROUPS	Initial paw thickness (mm)	Paw thickness on 3 hrs. (mm)	Increase in paw thickness (mm)	% of inhibition
Control	1.83±0.11	2.9±0.1	1.07±0.1	.....
Vehicle control	1.84±0.07	2.86±0.1	1.02 ± 0.054^{ns}	4.6%
Standard	1.88±0.054	2.46±0.05	0.58±0.054***	45.79%
NMC15 (25 mg/kg b.wt)	2.0±0.083	2.72±0.044	0.72±0.044**	32.71%
NMC15 (50 mg/kg b.wt)	1.95±0.081	2.55±0.057	0.7±0.057***	34.57%

Values are expressed as mean ± SD for 6 animals in each group. P<0.001***, P<0.01**, ns – non-significant.

Fig. 4.53 Effect of sample NMT07 on carrageenan-induced acute inflammation in reducing the paw edema in Swiss albino mice.

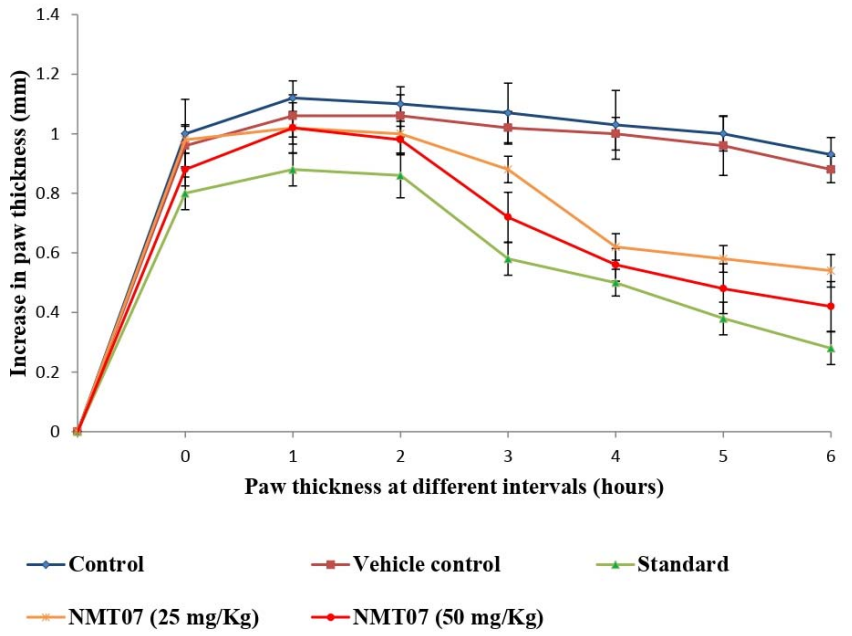

Table 4.26 Inhibition of carrageenan- induced acute inflammation by NMT07 extract.

GROUPS	Initial paw thickness (mm)	Paw thickness on 3 hrs. (mm)	Increase in paw thickness (mm)	% of inhibition
Control	1.83±0.11	2.9±0.1	1.07±0.1	.....
Vehicle control	1.84±0.07	2.86±0.1	1.02±0.054^{ns}	4.6%
Standard	1.88±0.054	2.46±0.05	0.58±0.054***	45.79%
NMT07 (25 mg/kg b.wt)	1.8±0.044	2.68±0.044	0.88±0.044*	17.75%
NMT07 (50 mg/kg b.wt)	1.8±0.054	2.50±0.083	0.70±0.083***	37%

Values are expressed as mean ± SD for 6 animals in each group. P<0.001***, P<0.05*, ns – non-significant.

4.9.2.2 Inhibition of formalin-induced inflammation

The sample NMC15 and NMT07 extracts were found to be effective in reducing chronic inflammation induced by formalin. In the case of NMC15 treated animals, percentage inhibition for 25 and 50 mg/kg b.wt. was 20.23 and 32.14 % (Table 4.27 and Fig. 4.54). The sample NMT07 extract administration also reduced formalin-induced inflammation with percentage inhibitions of 26.19 and 40.47 % for 25 and 50 mg/kg b wt. Diclofenac-treated animals at 10 mg/kg b. wt. showed 58.33% inhibition (Table 4.28 and Fig. 4.55).

Fig. 4.54 In vivo anti-inflammatory effect of sample NMC15 on formalin- induced chronic inflammation edema of Swiss albino mice.

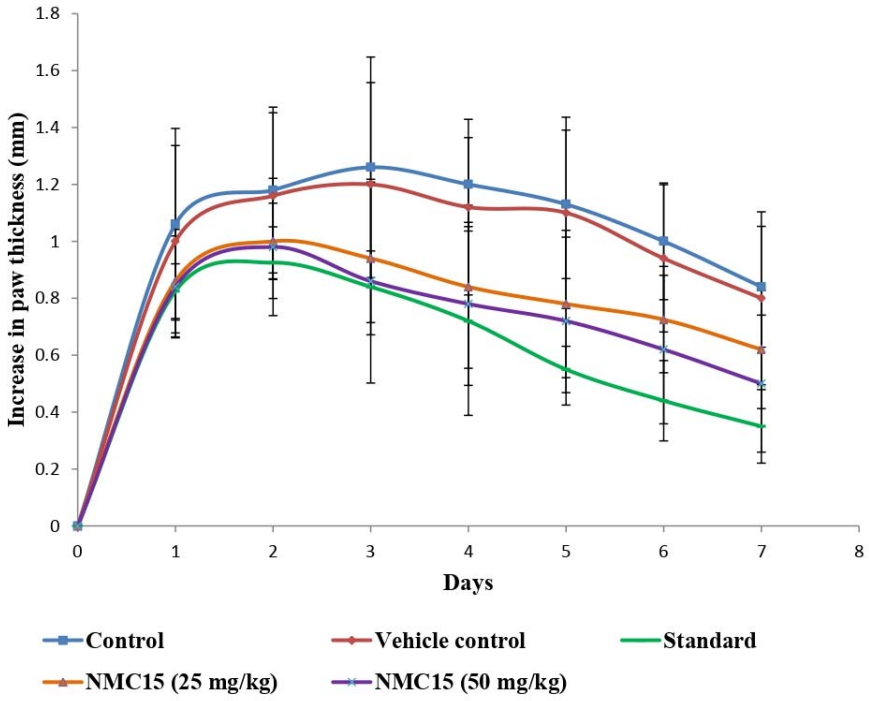

Table 4.27 Inhibition of formalin-induced chronic inflammation by NMC15 extract.

GROUPS	Initial paw thickness (mm)	Paw thickness on 7th day (mm)	Increase in paw thickness (mm)	% of inhibition
Control	1.84±0.336	2.68±0.212	0.84±0.204	.....
Vehicle control	1.96±0.336	2.76±0.303	0.8 ± 0.258^{ns}	4.76%
Standard	1.92±0.095	2.27±0.129	0.35±0.141***	58.33%
NMC15 (25 mg/kg b.wt)	1.77±0.298	2.44±0.251	0.67±0.330**	20.23%
NMC15 (50 mg/kg b.wt)	1.75±0.129	2.32±0.125	0.57±0.25***	32.14%

Values are expressed as mean ± SD for 6 animals in each group. P<0.001***, P<0.01**, ns – non-significant.

Fig. 4.55 In vivo anti-inflammatory effect of sample NMT07 on formalin-induced chronic inflammation edema of Swiss albino mice.

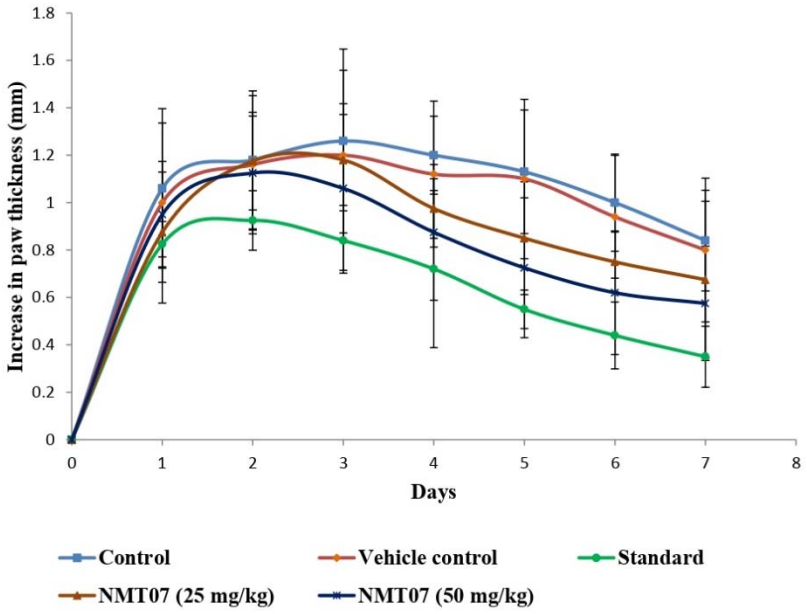

Table 4.28 Inhibition of formalin-induced chronic inflammation by NMT07 extract

GROUPS	Initial paw thickness (mm)	Paw thickness on 7th day (mm)	Increase in paw thickness (mm)	% of inhibition
Control	1.84±0.336	2.68±0.212	0.84±0.204	.....
Vehicle control	1.96±0.336	2.76±0.303	0.8 ± 0.258^{ns}	4.76%
Standard	1.92±0.095	2.27±0.129	0.35±0.141***	58.33%
NMT07 (25 mg/kg b.wt)	1.94±0.181	2.56±0.207	0.62±0.187**	26.19%
NMT07 (50 mg/kg b.wt)	1.96±0.178	2.46±0.240	0.50±0.260***	40.47%

Values are expressed as mean ± SD for 6 animals in each group. P<0.001***, P<0.01**, ns – non-significant.

4.9.3 Anticancer study

4.9.3.1 EAC-induced ascites tumor model

All the animals injected intraperitoneally with EAC cells developed ascites tumors. The control and vehicle control groups survived only for an average of 17.2 ±2.16 and 18.0 ±1.67 days, respectively. But the cyclophosphamide administered group survived for an average of 27.6 ±2.06 days and the % increase in lifespan was found to be 60.46% when compared to control animal groups. The NMT07 extract at 25 and 50 mg/kg b.wt. exhibited a mean survival days of 22.0 ±1.22 and 26.6 ±2.30 days, respectively. The higher dose shows 54.65% increase in lifespan whereas lower dose only 27.90% as shown in table 4.30 and fig. 4.56.

Fig. 4.56 EAC- induced ascites tumor in mice

Table 4.29 Showing the number of EAC- bearing mice that survived in each group.

GROUPS	DAYS									
	3	**6**	**9**	**12**	**15**	**18**	**21**	**24**	**27**	**30**
Control	6	6	6	6	6	5	3	0	0	0
Vehicle control	6	6	6	6	6	4	2	0	0	0
Standard	6	6	6	6	6	5	4	4	2	0
NMT07 (25 mg/kg)	6	6	6	6	6	5	4	2	0	0
NMT07 (50 mg/kg)	6	6	6	6	6	6	5	4	1	0

Table 4.30 The mean survival days and percent increase in lifespan of EAC-bearing mice.

Groups	Mean Survival Days	% ILS
Control	**17.2 ±2.16**	**……..**
Vehicle control	**18.0 ±1.67^{ns}**	**4.65**
Standard	**27.6 ±2.06*** **	**60.46**
NMT07 (25 mg/kg)	**22.0 ±1.22** **	**27.90**
NMT07 (50 mg/kg)	**26.6 ±2.30*** **	**54.65**

Values are expressed as mean ± SD for 6 animals in each group. P<0.001***, P<0.01**, ns – non significant.

Fig.4.57 Effect of sample NMT07 on survival pattern of ascites tumor- bearing mice.

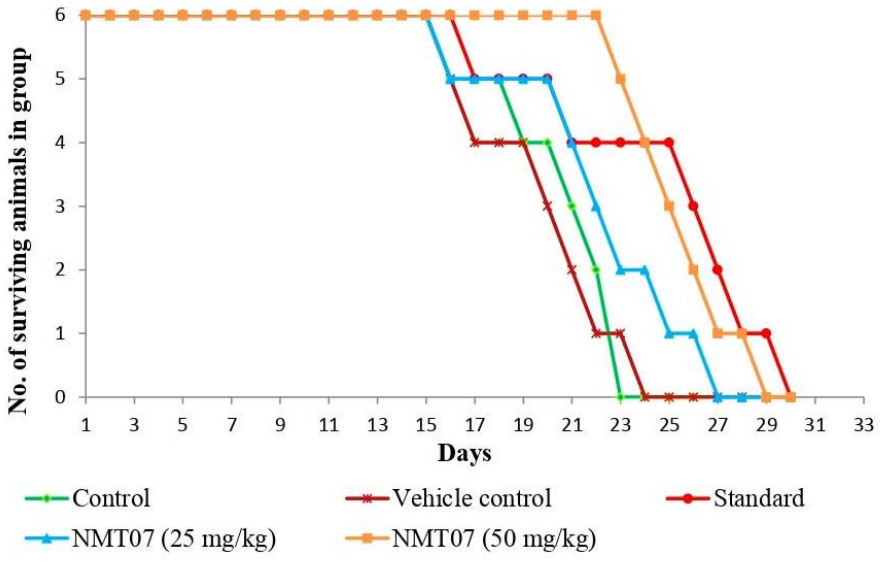

4.9.3.2 DLA-induced solid tumor model

All the animals injected intramuscularly with DLA cells on the right hind limb have developed visible solid tumors by the 6th day of tumor induction and were found to increase day by day, as in fig. 4.58. The tumor volume in the extract-treated group at different weeks intervals was decreased compared to the control group of animals. The treatment of extract of varying concentration, higher dose (50 mg/kg b.wt.), lower dose (25 mg/kg b.wt.) and standard (10 mg/kg b.wt.) for 10 consecutive days after tumor development showed 78.97% ($P<0.001$), 29.34%, and 85.72% ($P<0.001$) tumor growth regression, respectively as compared to control (Table 4.31).

Table 4.31 Antitumor effect of NMT07 on DLA solid tumor.

Groups	**Tumor volume (cm^3) on 5th week**	**% inhibition**
Control	4.175 ±0.754	.....
Cyclophosphamide (10 mg/kg)	0.596 ±0.445***	85.72%
NMT07 (25 mg/kg)	2.95 ±0.410^{ns}	29.34%
NMT07 (50 mg/kg)	0.878 ±0.456***	78.97%

Values are expressed as mean ± SD for 6 animals in each group. $P<0.001$***, ns – non significant.

Fig.4.58 Effect of NMT07 extract on DLA induced solid tumor development in mice.

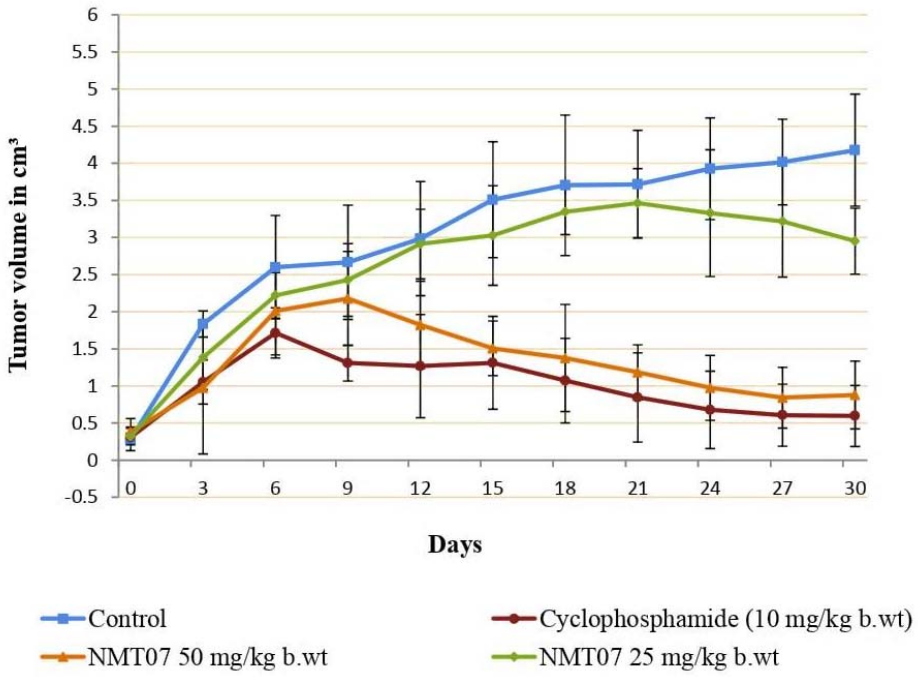

4.9.3.3 Hematological parameters

The hemoglobin content for normal control, standard, and higher dose are 14.45 ±0.21, 13.35 ±0.21, and 13.05 ±0.21 g/dL, respectively found to be similar in comparison with tumor control (10.70 ±0.42 g/dL) and lower dose (11.30 ±0.42 g/dL). The RBC and WBC for normal control, standard, a lower dose and higher dose have no differences in addition to tumor control (5.40 $x10^6$/µL ±0.35). The WBC for normal control (4.7$x10^3$/µL ±0.14) in comparison with a standard (7.0$x10^3$/µL ±0.42), a lower dose (16.7x103/µL ±0.35) and higher dose (10.4$x10^3$/µL ±0.56) has no differences in addition to tumor control (42.2$x10^3$/µL ±0.56). The study points out that there is no statistical difference while assessing hematological parameters with standard and higher dose drugs compared to normal control. But tumor control and lower dose drug groups showed statistically significant differences with the normal control (Table 4.32).

Table 4.32 Hematological parameters of DLA tumor-bearing mice on the 30th day.

Treatment	**Hb (g/dl)**	**RBC (1x10^6/µL)**	**WBC (1x10^3/µL)**	**Neutrophils (%)**	**Lymphocytes (%)**	**Platelets (1x10^3/µL)**
Normal control	14.45 ±0.21	6.65 ±0.35	4.7 ±0.14	36.5 ±2.12	56.0 ±2.82	435 ±0.35
Tumor control	10.70 ±0.42***	5.40 ±0.35*	42.2 ±0.56***	18.5 ±0.70***	79.0 ±1.41***	1050 ±0.28***
Standard	13.35 ±0.21*	6.05 ±0.28	7.0 ±0.42*	31.0 ±1.41	67.5 ±0.70**	715 ±0.35**
NMT07 (25 mg/kg)	11.30 ±0.42***	5.80 ±0.28	16.7 ±0.35***	18.0 ±1.41***	77.0 ±2.82***	850 ±0.28***
NMT07 (50 mg/kg)	13.05 ±0.21*	5.90 ±0.41	10.4 ±0.56**	27 ±2.82*	70.5 ±2.12**	780 ±0.56***

Hb: Hemoglobin; **RBC**: Red Blood Cells; **WBC**: White Blood Cells. Values are expressed statistically as mean ± SEM; *P < 0.05, **P < 0.01, ***P < 0.001 compared to normal control.

4.9.3.4 Histopathology of tumor

Histopathology of tumor-induced mice in different groups showed a varied number of inflammatory cells as described and shown below:-

Fig. 4.59 Macroscopic view of variation in tumor size of mice in different groups.

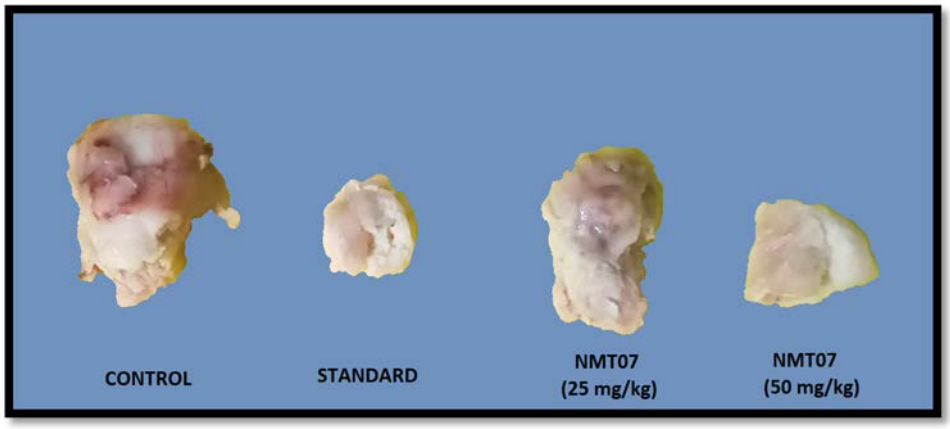

Fig. 4.60 DLA-induced tumor macroscopy and microphotography of control mice.

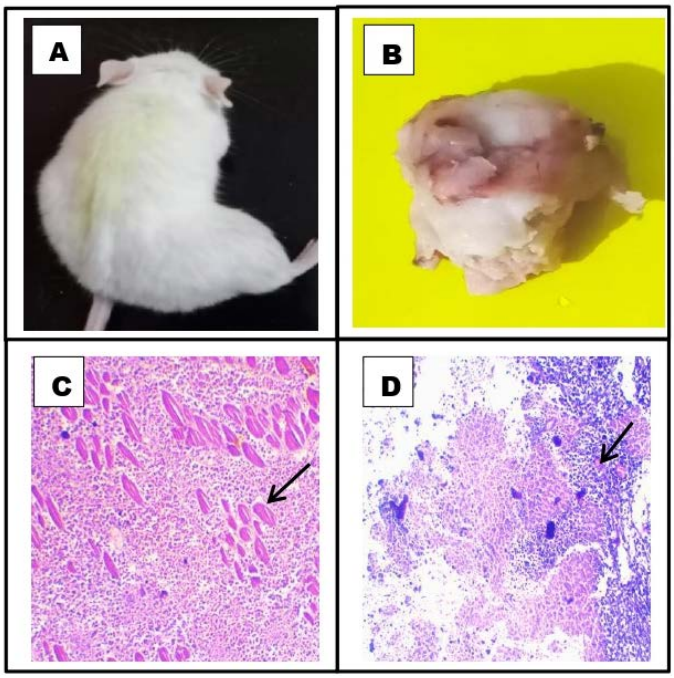

A- Solid tumor bearing control mice.

B- Dissected tumor macroscopy.

C- Necrotic muscle fibers (arrow) due to infiltration of neoplastic cells.

D- More necrotic cells (arrow) visualized using haematoxylin and eosin stain.

Fig. 4.61 DLA- induced tumor macroscopy and microphotography of Cyclophosphamide-treated mice.

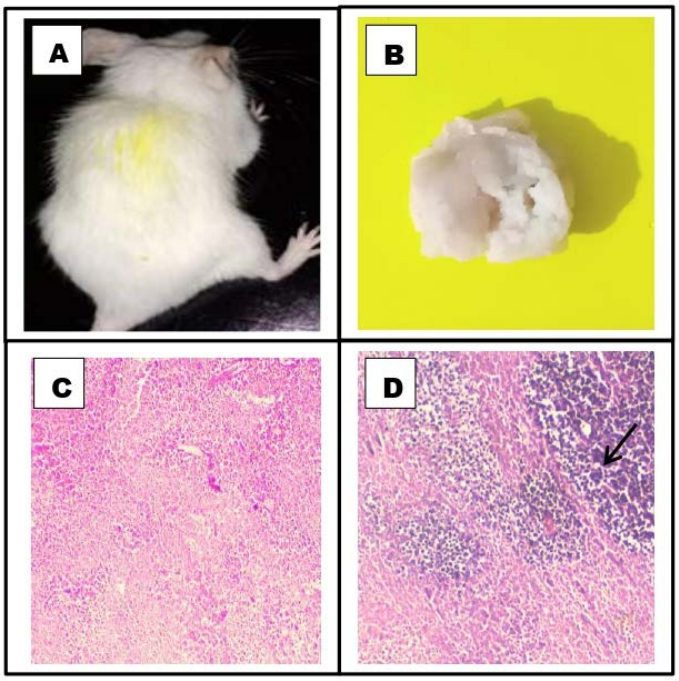

A- Solid tumor bearing cyclophosphamide- treated mice.

B- Dissected tumor macroscopy.

C- Normal cells (pink colour).

D- Less necrotic cells (arrow) among the normal cells.

Fig. 4.62 DLA-induced tumor macroscopy and microphotography of lower dose of NMT07 extract-treated mice.

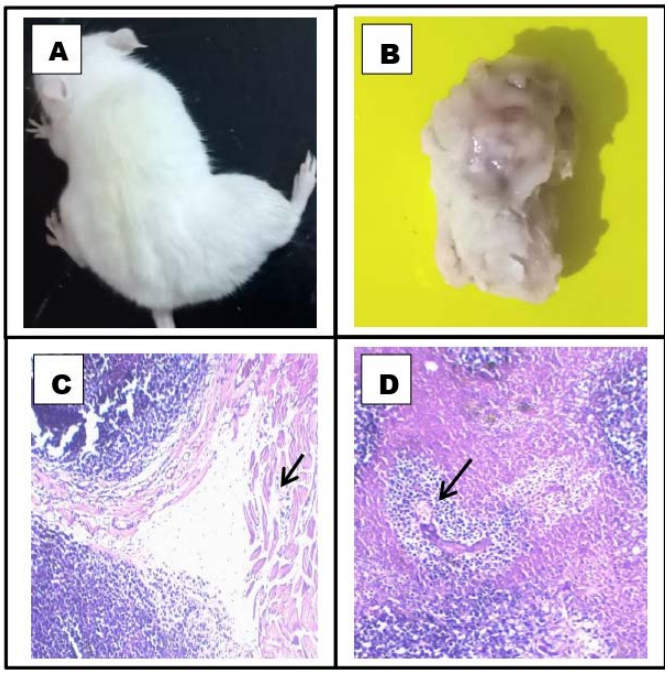

A- Solid tumor bearing lower dose NMT07 extract-treated mice.

B- Dissected tumor macroscopy.

C- More infiltration of neoplastic cells in the underlying muscles leads to necrotic muscle fibers (arrow).

D- Tumor angiogenesis due to inflammation seen dispersed in necrotic cells (arrow).

Fig. 4.63 DLA-induced tumor macroscopy and microphotography of higher dose of NMT07 extract-treated mice.

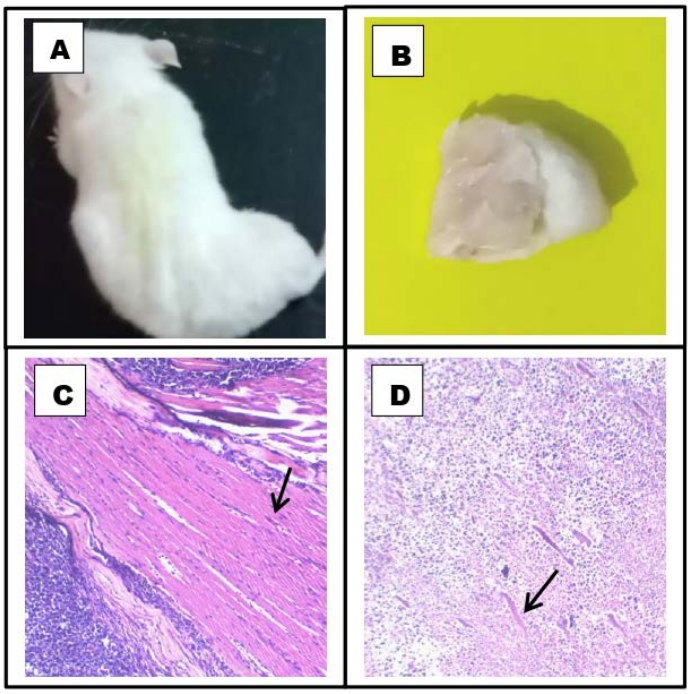

A- Solid tumor bearing higher dose NMT07 extract- treated mice,

B- Dissected tumor macroscopy,

C- Less infiltration and muscle fibers normal (arrow),

D- Less necrotic muscle cells (arrow) among the normal cells.